DEVELOPMENT OF ONLINE OXIDE ION SENSOR FOR CONTINUOUS MONITORING OF MOLTEN NITRATE SALTS FOR SOLAR ENERGY POWER PLANTS

by

Aliaksei Minko

A thesis submitted to the faculty of
The University of Utah
in partial fulfillment of the requirements for the degree of

Master of Science

in

Nuclear Engineering

Department of Civil and Environmental Engineering

The University of Utah

May 2018

The University of Utah Graduate School

STATEMENT OF THESIS APPROVAL

The thesis of **Aliaksei Minko**

has been approved by the following supervisory committee members:

Michael F. Simpson	, Chair	**06/07/2016** Date Approved
Tatjana Jevremovic	, Member	**05/27/2016** Date Approved
Azaree T. Lintereur	, Member	**05/31/2016** Date Approved

and by **Michael Ernest Barber** , Chair/Dean of

the Department/College/School of **Civil and Environmental Engineering**

and by David B. Kieda, Dean of The Graduate School.

ABSTRACT

Molten salts, particularly nitrates and nitrites, have been used in concentrated solar power (CSP) plants as a heat transfer fluid (HTF) since the early 1980s. One of the main issues associated with the use of molten salts is their decomposition at high temperatures. Currently, there is no technology available for the continuous monitoring of the composition of these salts. This study focuses on the research and development of an online oxide ion sensor that would provide CSP plant operators with live data.

The formation of an oxide ion is an indication of the decomposition of nitrate and nitrite salts. Electrochemical methods like cyclic voltammetry (CV), linear square voltammetry (LSV), and square wave voltammetry (SWV) were used to measure changes in the O^{2-} concentration in both HITEC and Solar Salt. The peak current values measured with LSV and SWV were correlated via a linear function to the oxide ion concentration. Multiple calibration curves were developed for both salts in bench scale electrochemical experiments.

A variety of electrochemical test methods and test materials were investigated in this project to support the development of a real-time sensor for oxide ions in molten nitrate salts. Platinum coated titanium rods were used as the working (WE) and counter electrodes (CE). A $Ag/AgNO_3$ electrode contained inside of a thin-walled mullite tube served as a reference electrode. The probe designed and assembled based on this study performed effectively to measure the change in oxide concentrations.

To my parents,
Aliaksandr and Elina Minko,
And all my friends and family,
For their endless love, support, and patience.

TABLE OF CONTENTS

LIST OF TABLES

LIST OF FIGURES

ACKNOWLEDGEMENTS

I cannot express how grateful I am to everyone who has been involved in this project and made this thesis possible. Below are some of the people, whose contributions have been extremely important:

- Dr. Michael Simpson for his support, constant advice, and expert guidance.
- Dr. Sang-Mun Jeong for his help in the development of the electrochemical setup.
- Dr. Mark Anderson, Paul Brooks and Michael Zupan at the University of Wisconsin for their help and hospitality.
- Dr. Tatjana Jevremovic, Dr. Azaree Lintereur, and Dr. Luther McDonald for their advice and assistance.
- Abengoa Solar and Dylan Grogan for their financial support and advising.
- My current and past colleagues: Devin Rappleye, Adam Burak, Avi Jurovitzki, Chao Zhang, Cristina Bahamonde, David Horvath, Ian Schwerdt, Lauryn Hansen, Mario Gonzalez, Milan Stika, Parker Okobee, and Prashant Bagri.

CHAPTER 1

INTRODUCTION

1.1 Overview of Solar Energy

Mankind has always used the energy of the sun in one way or another. Greeks and Romans used mirrors to light torches for religious purposes during the 3rd century B.C [1]. In 1839, Edmond Becquerel demonstrated the photovoltaic effect while illuminating platinum electrodes coated with silver chloride or silver bromide inserted into acidic solution [2]. In 1860, Augustin Mouchot started experimenting with solar cooking devices. He worked on the development of solar power steam engines between 1860 and 1880. In 1866 his first sun-powered engine with a reflector was presented to the French Emperor Napoleon III who provided Mouchot with financial support to build an industrial model [3]. In 1876, William Grylls Adams and Richard Day exposed a selenium bar with platinum contacts to sunlight and produced electricity. Charles Fritz invented the first selenium-based solar cell in 1883. Designs similar to Fritz's were used until 1940's [1,2]. Calvin Fuller, Gerald Pearson, and Daryl Chapin presented the silicon solar cell in 1954 while working at Bell Laboratories [4]. By the early 1970s solar cells became pretty common in toys and electronics. During the 1970's Energy Crisis, the Department of Energy started funding solar power research in the United States [5]. And only in recent decades has the world started using this renewable energy source for

commercial or residential production of electricity.

Today, solar power is collected via two different pathways. The sunlight is converted into electricity either directly via photovoltaics (PV), or indirectly – using concentrated solar power (CSP). PV systems offer modularity and simplicity of installation, while CSP systems are usually large-scale power plants that are designed to last for decades and sustainably deliver power to the grid.

In February 2011, the U.S. Department of Energy (DOE) Solar Energy Technologies Office announced the SunShot program that focuses on making solar energy cost competitive with other forms of electricity by the end of the decade. It was estimated that the price of $0.06 per kilowatt-hour would make solar electricity cost-competitive with other more traditional sources of electricity. According to SunShot's estimates, this price can be achieved by 2020 with CSP systems [6]. Figure 1.1 shows the current and projected costs of CSP.

1.2 Review of Concentrated Solar Power (CSP) Systems

Three types of CSP systems are reviewed here—parabolic trough systems, power tower systems, and dish/engine systems. They are described in some detail below.

1.2.1 Parabolic Trough Systems

Parabolic trough systems are the most common type of CSP systems in the U.S. These systems use arrangements of parabolic mirrors to collect the solar energy. The sunlight is reflected and focused on a receiver tube that carries a heat transfer fluid. It is pumped through the heat exchangers to create superheated steam that spins the turbine

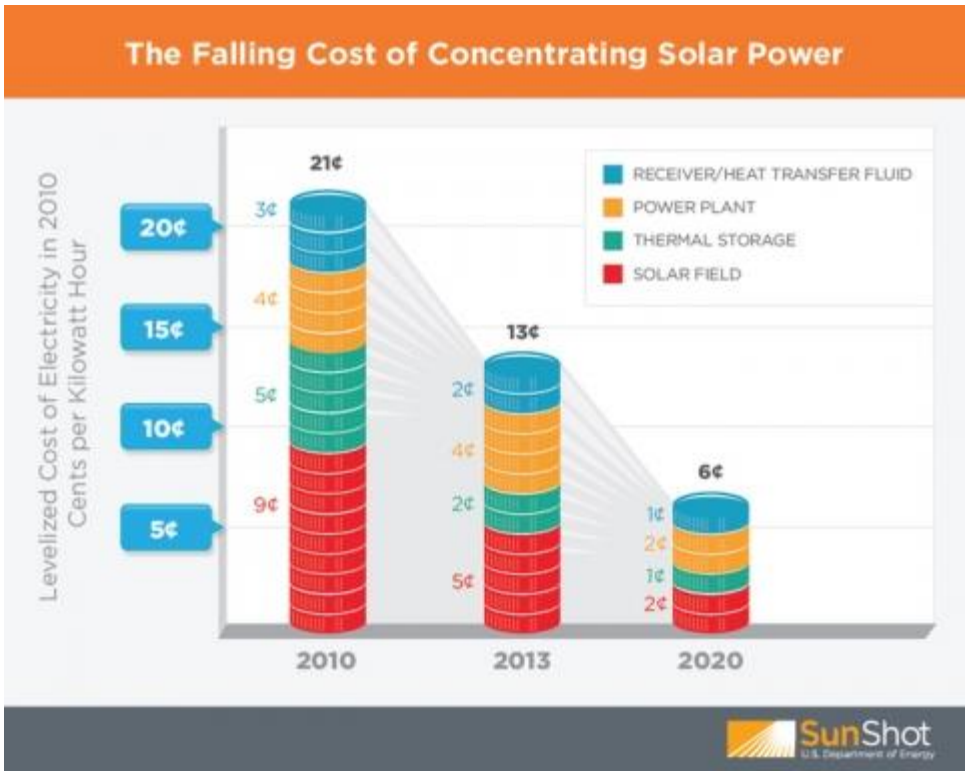

Figure 1.1. Projected cost of electricity produced with CSP technologies. Adapted from [6]

and drives the generator to produce electricity. The steam leaving the turbine is then condensed using conventional methods and recycled in the system. If water is used as a working fluid, the steam can be generated directly in the solar field. Figure 1.2 shows the sketch of the cycle and a corresponding P-V diagram. All 4 steps of the cycle are clarified in Table 1.1.

Typical parabolic trough power plants consist of multiple large collector fields. Each collector field has a large number of parallel collectors aligned in a north-south orientation with a single-axis tracking system that rotates the parabolic mirror and keeps the focal point on the receiver while the sun moves from east to west during the day. Typical schematic of parabolic trough power plant is shown in Figure 1.3.

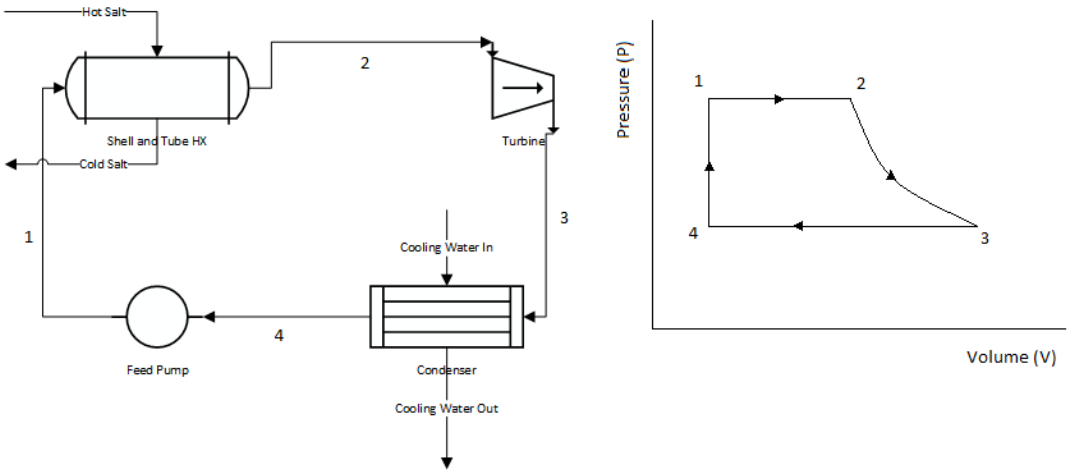

Figure 1.2. Rankine cycle and a corresponding P-V diagram

Table 1.1. Main steps of the Rankine cycle

Process Step	**Process Description**
1-2	Isobaric heat transfer
2-3	Isentropic expansion
3-4	Isobaric heat rejection
4-1	Isentropic compression

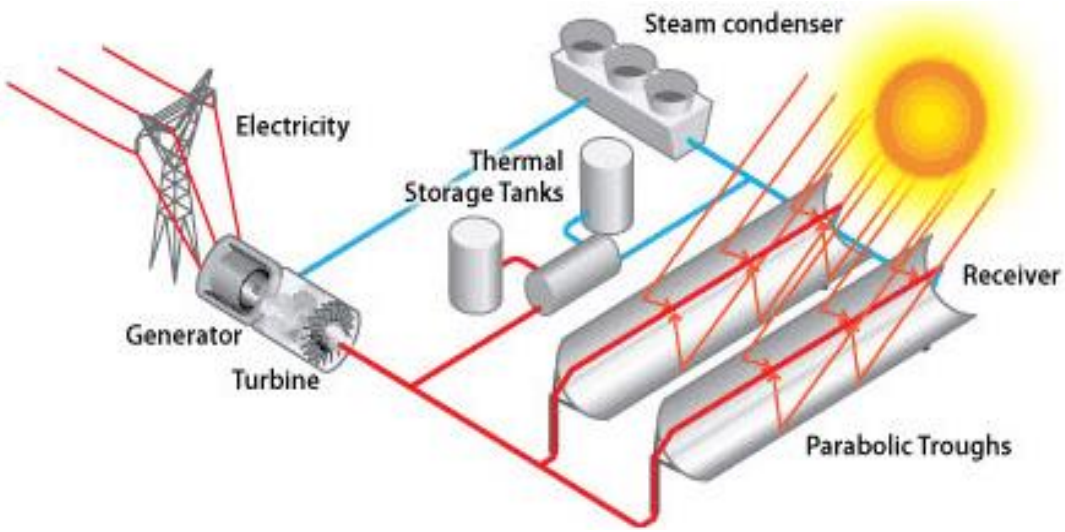

Figure 1.3. A linear concentrator power plant using parabolic trough collectors. Adapted from [7]

1.2.2 Power Tower Systems

Power tower concentrating solar power systems use large flat mirrors called heliostats to focus the sunlight onto a receiver on top of the tall tower as seen in Figure 1.4. Just like with parabolic trough systems, the heat transfer fluid in the receiver is used to generate steam that is used in the conventional turbine generator. The heliostats in power tower power plants have a two-axis tracking system to ensure the constant reflection of the sunlight onto the receiver regardless of the position of the sun. The main advantage of this system is the ability to achieve very high temperatures when a large field of heliostats focuses all of the energy on the single receiver. This allows the use of various heat transfer fluids. Individual commercial power plants could be designed to produce up to 377 MW of net electricity [8].

Today, Ivanpah Solar Power Facility in California is the world's largest and most well-known solar thermal power plant [9]. There are 300,000 computer-controlled heliostats that reflect the sunlight to boilers that sit atop three 459-foot tall towers. The

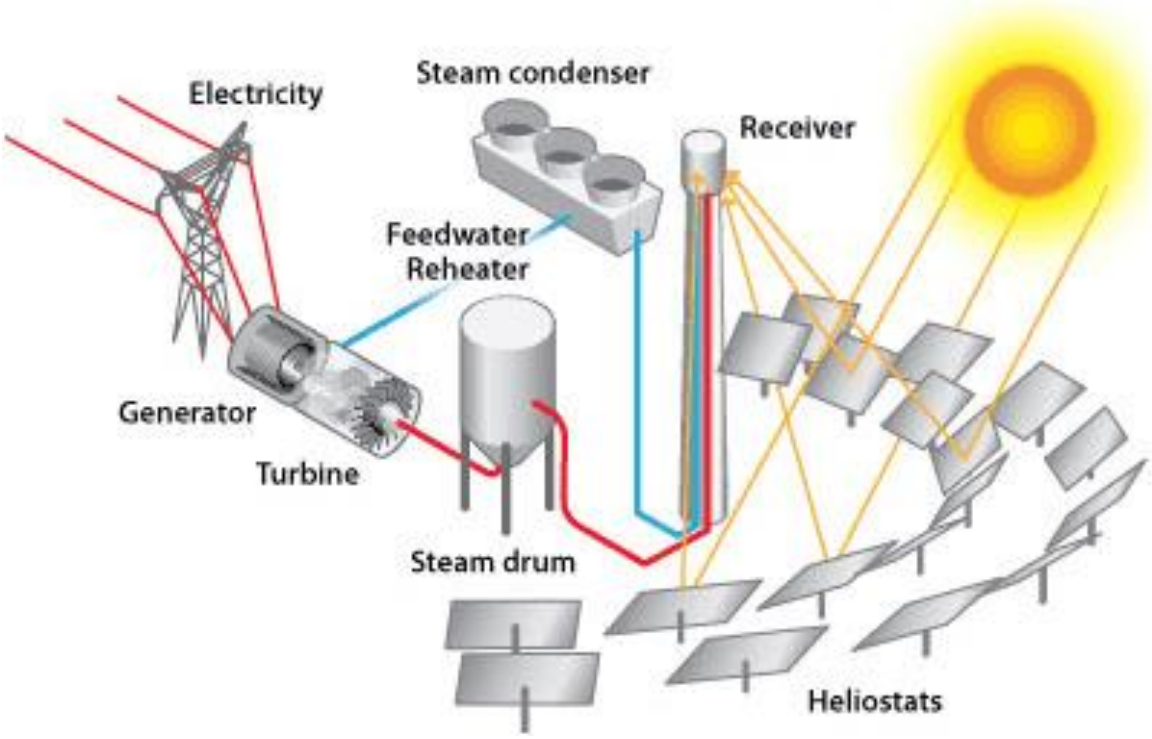

Figure 1.4. A power tower power plant. Adapted from [8]

plant occupies the area of 3500 acres and produces 377 MWe of net power. Ivanpah Solar Power Facility uses water as their working fluid. Since water cannot be used to effectively store energy, natural gas is used as a secondary fuel to keep the plant operational during the cloudy days and at night. In 2014, the state of California improved Ivanpah's request to increase annual natural gas consumption from 328 to 525 million of standard cubic feet [10].

1.2.3. Dish/Engine Systems

Dish/engine systems (also known as Stirling dish) use the parabolic dish of mirrors that concentrates the sunlight onto the power conversion unit. These dish systems are mounted on a structure that tracks the position of the sun throughout the day and

maximizes the amount of the sunlight reflected onto receiver. Figure 1.5 shows a typical dish/engine system.

The power conversion unit consists of a thermal receiver and an engine/generator. The thermal receiver is usually a bundle of tubes filled with a gas like helium that acts as a heat transfer fluid and a working fluid for the engine. A Stirling engine is normally used in these systems. It operates on a closed cycle in which the fluid heated by sun expands, moves the pistons, and then transfers back to the cold piston. The pistons rotate the crankshaft that drives the generator producing electrical power. Figure 1.6 shows the corresponding P-V diagram and all the steps are described in Table 1.2.

Dish/engine systems produce a small amount of electricity compared to other CSP technologies. However, they have the highest solar to electric energy conversion efficiency. These systems are expensive and are still being researched by industry, national laboratories, and universities. The Maricopa Solar power plant in Arizona successfully used 60 units with an overall capacity of 1.5 MWe [11].

1.3. Heat Transfer Fluids for CSP Plants

The choice of the heat transfer fluid largely depends on the type of the CSP plant and its design. The fluid carries the heat from the receivers and collectors to the heat exchanger and heat storage tanks. Optimization of the heat transfer fluid (HTF) can improve the thermal-to electricity energy conversion efficiency and lower the operating costs of the power plant. Thermal stability at high temperatures is particularly important to improve the efficiency of the energy conversion.

Options for the heat transfer fluid of a CSP plants are water, synthetic oils, and

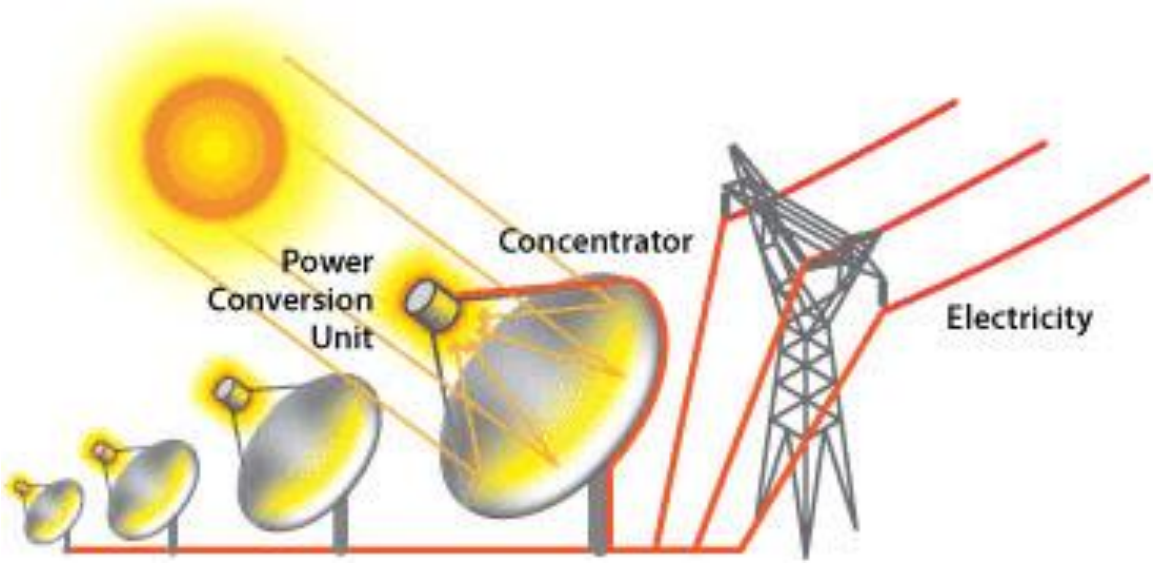

Figure 1.5. Dish/engine system. Adapted from [12]

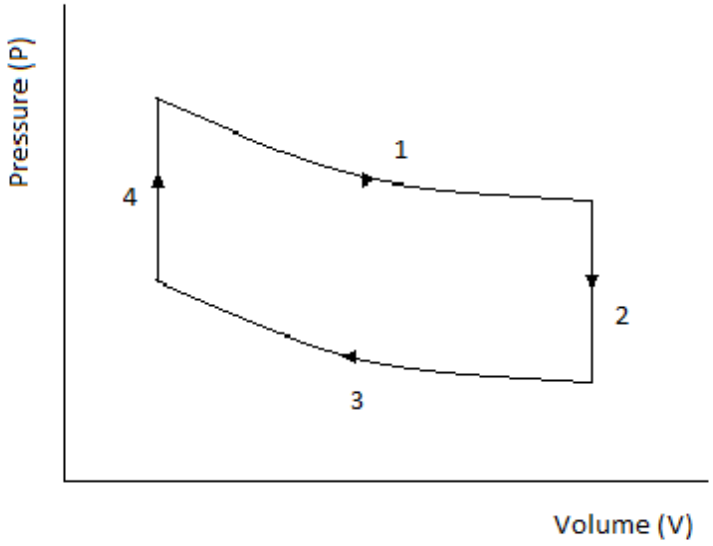

Figure 1.6. P-V diagram of the Stirling engine cycle

Table 1.2. Main steps of the Stirling cycle

Process Step	Process Description
1	Isothermal expansion
2	Isovolumetric heat removal
3	Isothermal compression
4	Isovolumetric heat addition

molten salts. The pros/cons of each fluid option are given in Table 1.3. Sometimes multiple different heat transfer fluids are used in different loops of the same plant, but that usually increases both initial and operating costs.

1.3.1 Molten Salts

As shown in Table 1.3, molten salts have a number of attractive characteristics that make them an excellent heat transfer fluid for CSP systems. The key attribute is their thermal stability at high temperatures. If the heat transfer fluid were to be heated by a solar field to 500 ºC, the efficiency of an attached Rankine cycle would go as high as 40% [13]. Because of their relatively low melting points, low cost, and minimal environmental impact, nitrate salts have been extensively investigated in the industry. Two nitrate salt mixtures of specific interest (HITEC and Solar Salt) are discussed below.

HITEC is a granular white salt (yellowish when melted) and consists of 7% of $NaNO_3$, 40 % of $NaNO_2$, and 53% of KNO_3 by weight. It is widely used in the industry because of its low melting point (142 ºC), high heat capacity, thermal stability, great fluid dynamics properties, and low cost [13]. Low melting point is a key property of the HTF,

Table 1.3. Comparison of popular heat transfer fluids

	Water	**Oil**	**Molten Salt**
Pros	• Simplicity • Low cost • Environmentally benign	• Medium thermal stability • High heat capacity	• Higher thermal stability • Environmentally benign • High heat capacity
Cons	• No energy storage ability • High pressures at high temperatures	• Environmentally hazardous • Flammable/explosive	• Unknown behavior at high temperatures • Corrosion

since process upsets can cause dips in the temperature, and recovering from a frozen line would be extremely difficult and costly for a CSP. Startup of the fluid flow would also be extremely difficult when using a high melting point salt.

HITEC has been cited to be stable at temperatures up to 535 ºC and can be used for many years [13,14]. At higher temperatures in closed systems the nitrite in HITEC slowly decomposes to nitrate via the following reaction [15]:

$$5NaNO_2 \rightarrow 3NaNO_3 + Na_2O + N_2 \quad (1.1)$$

When HITEC is used in an open system and is in contact in the air with temperatures above 454 ºC, nitrite is slowly oxidized to nitrate via this reaction [15]:

$$2NaNO_2 + O_2 \rightarrow 2NaNO_3 \quad (1.2)$$

Similar to HITEC, Solar Salt is white and slightly yellow in color when melted. It is a mixture of 60% of $NaNO_3$ and 40% of KNO_3 by weight. Like other molten nitrates, Solar Salt has great thermodynamic, heat transfer, and fluid dynamic properties. It also has a neutral pH when dissolved in water, thus making its disposal environmentally benign. It has a melting point of 221 ºC and is cited to be stable at temperatures up to 600 ºC [13].

At very high temperatures, nitrates start decomposing and forming nitrites [16,17]:

$$NaNO_3 \rightarrow NaNO_2 + \frac{1}{2}O_2 \quad (1.3)$$

When HITEC is used in an open system and is in contact in the air with temperatures above 454 ºC, nitrite is slowly oxidized to nitrate via this reaction [15]:

$$2NaNO_2 \rightarrow Na_2O + \frac{3}{2}O_2 + N_2 \quad (1.3)$$

This is an undesirable reaction for a number of reasons. For one, it is very important to keep the chemical composition of the salt constant to avoid the increase of the freezing point. For another reason, generation of oxides in the salt can lead to corrosion of the metallic pipes and vessels. Thus it is critical for a CSP to operate at temperatures sufficiently low enough to prevent these decomposition reactions from occurring. It is hypothesized that continuous monitoring of O^{2-} ion concentration in the salt can be a good indicator of the salt thermally degrading. Development of such a measurement method should lead to optimal process control of CSP systems to prevent damage to the salt while maximizing thermal energy conversion efficiency.

CHAPTER 2

LITERATURE REVIEW

2.1. Application of Molten Salt for Solar Power

For developing CSP plants with optimal average power output, it is necessary to find a suitable heat transfer fluid and develop new thermal energy storage systems—assuming that this approach is cheaper than installing backup natural gas-fueled power systems. Current operation temperatures of CSP plants are limited to less than 400 °C by organic oils [18]. Molten salts have been proven to increase the cycle efficiency of CSP plants and lower the levelized cost of electricity (LCOE) [6].

Reilly and Kolb [19] discuss the evolution of CSP technology in the U.S. The first CSP plant in the U.S., Solar One, was built near Barstow, California, and was operational from 1982-1988. Solar One was a power tower plant that used water as heat transfer fluid (HTF). It was converted to steam right in the receiver and used to power a Rankine cycle steam turbine. The beam of light was focused by 1818 heliostats each having a reflective are of 39.3 m^2. The plant successfully generated 10 MW_e for 8 h a day during the summer and 4 h a day during the wintertime. The project proved this technology very reliable. However, one of the biggest drawbacks was operation during the cloudy days. Since the turbine generator was connected to the receiver, even the passing clouds would interrupt the electricity supply to the grid. Solar One plant had a thermal storage system – the heat

was stored in a tank filled with rocks and sand (oil was used as the HTF). The design of the system was very complex and thermodynamically inefficient. While six years of Solar One's operation demonstrated the reliability of the power tower technology, it also raised issues with using water/steam as an HTF and having a better-designed thermal storage system.

In September 1994, the U.S. Department of Energy with an industry consortium began the construction of Solar Two. It was built on the same site as Solar Two and utilized many of its systems to minimize the capital investment. Solar Salt, a mixture of 60 wt % sodium nitrate and 40 wt % potassium nitrate, was chosen as the HTF for Solar Two. The choice of the new working fluid was supposed to eliminate two key issues of Solar One. First, new solar receiver was designed to improve the performance. Because water turned into a high-pressure steam in the old receiver, designers of Solar One had to use thick-walled tubes. Second, the oil/gravel/sand thermal storage did not perform adequately in Solar One. It consisted of multiple loops and heat exchangers where steam was heating the oil, which, in turn, was heating the sand-gravel storage. In addition to obvious heat losses due to complicated design, the oil's operating temperature was limited to 304^{o}C. At some point, Solar One also experienced a fire that seriously damaged the thermal storage system. All these issues were eliminated when the thermal storage system was redesigned. It consisted of two molten salt storage tanks – hot and cold. Molten salt left the receiver at 565^{o}C and flowed to the hot storage tank. Cold salt was held at 288^{o}C in the cold storage tank and was pumped straight to the receiver. Solar Two demonstrated the reliability of CSP plants and the use of molten salt as the HTF. It also showed that it is possible to supply solar power to the grid 24 h a day without

interruptions.

Bradshaw and Siegel [14] mentioned the fact that power plants at the scale of 100 MW require large quantities of heat transfer fluid. It is critically important for a CSP plant to continuously stay on grid and dispatch enough electricity to match peak demand. It was estimated that millions of kilograms of HTF are required for energy storage in 100 MW to 200 MW power plants. Currently, commercial parabolic trough plants use a synthetic oil, a mixture of diphenyl oxide and biphenyl oxide, as the HTF in collector fields. It offers a combination of low melting point and high upper temperature limit. However, to operate properly, commercial CSP plants are expected to have a thermal storage system and cost becomes an important factor in the choice of the HTF. Molten salt can minimize the investment cost and maximize the performance of the HTF. A recent study estimated the price of Solar Salt at $0.50 per kg and the price of organic oils at $3 to $4 per kg [20].

2.2. Thermal Stability of Molten Nitrates and Nitrites

Despite the promising properties of most nitrates, there are still thermal stability limitations associated with all salts. According to Kramer [16], mass losses with gas evolution are observed at higher temperatures due to three mechanisms. First, nitrite formation in the melt with oxygen release:

$$NaNO_3 \leftrightarrow NaNO_2 + \frac{1}{2}O_2 \tag{2.1}$$

Second, formation of alkali metal oxide with release of gaseous oxygen and nitrogen:

$$NaNO_3 \leftrightarrow Na_2O + \frac{5}{2}O_2 + N_2 \tag{2.2}$$

And finally, vaporization of nitrate salts:

$$NaNO_3\ (l)\ \leftrightarrow\ NaNO_3\ (g) \tag{2.3}$$

This report also discusses the experimental results obtained during the study of thermal stability. Using thermogravimetry and mass spectrometry, activation energies for decompositions of sodium nitrate, potassium nitrate, and sodium nitrite in vacuum were obtained and compared to some previous findings. Table 2.1 summarizes the findings.

Bradshaw and Siegel [14] confirm that partial dissociation of nitrate ion to nitrite ion is the primary reaction in the decomposition of the binary Solar Salt mixture. At operating temperatures around 500 °C the shift from nitrate to nitrite occurs slowly and is limited by the partial pressure of oxygen in the atmosphere. This work also discusses the use of molten salts with substantial concentrations of nitrite ions, such as HITEC. The major advantage of these salts is their low melting temperatures. However, salts with high amount of nitrites undergo the reverse reaction (Equation 2.1) when in contact with oxygen. This could lead to an increasing concentration of nitrates and increasing melting

Table 2.1. Activation energies for decomposition of $NaNO_3$, KNO_3, and $NaNO_2$. Modified from [16]

Salt	Activation Energy, Kcal/mole	Process	Reference
$NaNO_3$	44	Decomposition in Air	[21]
$NaNO_3$	41	Vaporization	[23]
$NaNO_3$	36	Decomposition in Vacuum	[16]
KNO_3	65	Decomposition in Air	[22]
KNO_3	42	Vaporization	[24]
KNO_3	35	Decomposition in Vacuum	[16]
$NaNO_2$	43	Decomposition in Air	[21]
$NaNO_2$	32	Decomposition in Vacuum	[16]

point, which is a concern in large trough receiver systems.

Similarly to nitrates, nitrites might decompose at high temperatures to yield oxide, peroxide and superoxide ions [25]. Generally, decomposition occurs via the following reaction:

$$2NO_2^- \leftrightarrow O^{2-} + \frac{3}{2}O_2 + N_2 \quad (2.4)$$

Oxide ions in the melts also react with atmospheric CO_2 [26]. According to Bradshaw, carbon dioxide will convert oxide ion to carbonate via this reaction:

$$CO_2 + O^{2-} \leftrightarrow CO_3^{2-} \quad (2.5)$$

Picard et al. [27] mentions that thermochemical decomposition of nitrates [28,29] and nitrites [30,31,32] has been a subject of multiple studies, but the researchers do not agree about the reactions that take place. It is fairly clear, however, that the decomposition is always accompanied by the release of oxygen, nitrogen, nitrogen oxides, and the production of alkali oxide.

2.3. Electrochemistry of Molten Nitrates and Nitrites

In order to control the thermal stability of the salt, it is necessary to monitor the concentrations of oxide ions in the salt. Voltammetric analysis using a set of electrodes immersed in the molten salt could in theory be used for this purpose. Multiple such voltammetric methods could be used including but not limited to cyclic voltammetry (CV), linear sweep voltammetry (LSV), and square wave voltammetry (SWV).

Electrochemical experiments with molten sodium nitrate and nitrite mixtures were discussed by Picard et al. [27]. This work focused on the influence of pO^{2-} and temperature on decomposition of nitrate/nitrite mixtures. The relationship was

determined by measuring the equilibrium potential with a platinum electrode and measuring pO^{2-} with an yttria-stabilized zirconia membrane (as an indicator electrode). The study also mentions an important electrochemical reaction for the redox couple:

$$NO^{3-} + 2e^{-} = NO^{2-} + O^{2-} \quad (2.6)$$

And two more reactions with high equilibrium potentials that involve evolution of NO gas:

$$NO_2^{-} + e^{-} = NO(g) + O^{2-} \quad (2.7)$$

$$NO_3^{-} + 3e^{-} = NO(g) + 2O^{2-} \quad (2.8)$$

Work published by Choi et al. [33] showed that SWV may be the best approach to measure the concentration of oxide ions. In this study, SWV was used to monitor the concentration of oxide ions during the electrochemical reduction of UO_2 in molten Li_2O-LiCl at 650^{o}C. Multiple square wave voltammograms were developed by adding 0.00 to 0.77 wt % of Li_2O to LiCl. All the experiments were done in a high-purity argon atmosphere glovebox. Salt was melted in MgO crucible and maintained at 650^{o}C. An electrochemical cell was designed with a platinum wire working electrode, Li-Pb reference electrode, and a nickel rod as a counter electrode. The results of these studies indicated that the peak current increases with increasing concentration of O^{2-}.

Similar study was done by Massot et al. [34] where various amounts of Li_2O (from 0 to 0.0471 mol O^{2-}/kg) were added to LiF/NaF eutectic melts at 800^{o}C. The experiments were also performed under an inert argon atmosphere with salt melt in a glassy carbon crucible. Electrochemical probe consisted of a gold wire working electrode, glassy carbon counter electrode, and platinum wire that acted as a quasi-reference electrode $Pt/PtO_x/O^{2-}$ [35]. After a series of experiments, a linear relationship between peak current

and oxide concentration was observed.

Iizuka et al. [36] applied SWV to measure actinide concentrations in molten salt electrolytes. $PuCl_3$ was added to a molten LiCl-KCl eutectic mixture with concentrations ranging from 0.14 to 3.35 wt % of Pu. Again, all experiments were carried out in a high purity argon atmosphere glove box. About 50 g of LiCl-KCl eutectic mixture was melted in high purity alumina crucible. The probe was made with a tungsten wire working electrode, coiled tantalum wire counter electrode, and a reference electrode made up of a silver wire in a thing Pyrex glass tube with 1 wt % AgCl in LiCl-KCl. In this study, peak current increased with increasing the amount of $PuCl_3$ added, however the relationship was not linear.

Thus, this SWV appears to be applicable to a wide range of oxide ion concentrations of interest. But CV and LSV are standard electrochemical test methods that are almost always used to initially characterize the electrolyte. Using each method, calibration curves unique to HITEC and Solar Salt needed to be developed, and optimization of the square wave voltammetry method was needed. These were the primary objectives of this thesis project.

CHAPTER 3

EXPERIMENTAL SYSTEM AND METHODS

3.1 General Equipment

3.1.1 Inert Atmosphere Glovebox and a Chiller

Experiments were conducted in high temperature electrochemical cells operated in a glove box with inert argon atmosphere (see Figure 3.1). The glovebox used was PureLab HE4 from Innovative Technologies. High purity argon was supplied to the glovebox at all times and the gas purification module continuously scrubbed out O_2 and H_2O. This allowed the operation in an argon atmosphere with O_2 and H_2O concentrations below 1 ppm at all times.

High temperature experiments with molten salts inside of the glovebox require continuous cooling. Recirculation line of the glovebox is coupled with a heat exchanger to keep argon at the desired temperature. A PolyScience WhisperCool^{TM} chiller was used for recirculation of the coolant. For operation at or below 20°C, this chiller requires an antifreeze solution. Laboratory grade ethylene glycol and distilled water in a 50/50 mixture were used to allow operation at temperatures as low as -15°C. The glovebox has to be maintained at temperatures below 100°F at all times to avoid damage of rubber seals and gloves.

Figure 3.1. Glovebox and chiller used for experiments

3.1.2 Potentiostat

An Autolab PGSTAT302N potentiostat/galvanostat was used for all electrochemical experiments. Figure 3.2 shows that the potentiostat was configured (S) by connecting its leads in a 3-electrode setup. In this configuration, the sense electrode is coupled with the working electrode (WE). Potentiostat accurately controls the voltage of the counter electrode (CE) against the working electrode. Then the potential difference between the working electrode and reference electrode (RE) is well defined.

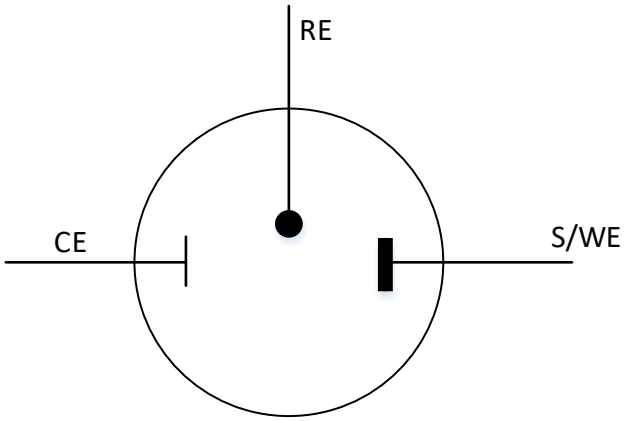

Figure 3.2. Schematic view of the 3-electrode setup

3.1.3 Simultaneous Thermal Analyzer

To determine water content in the supplied salt and to determine the temperature at which decomposition initially occurs, thermal analysis was performed using a simultaneous thermal analyzer (STA). The STA features both thermogravimetric analysis (TGA) and differential scanning calorimetry (DSC). TGA measures mass change in a sample as the temperature is increased, and DSC measures heat flow to or from the sample. The former method is useful for both identifying mass change due to off-gas of moisture and mass change due to decomposition of the salt. DSC can verify each of these processes, as they are also detectable based on endothermic processes that can be detected using DSC. For these analyses, small salt samples (~30 mg) were placed in a small alumina crucible and was placed in a Q600 TGA/DSC instrument from TA Instruments (see Figure 3.3).

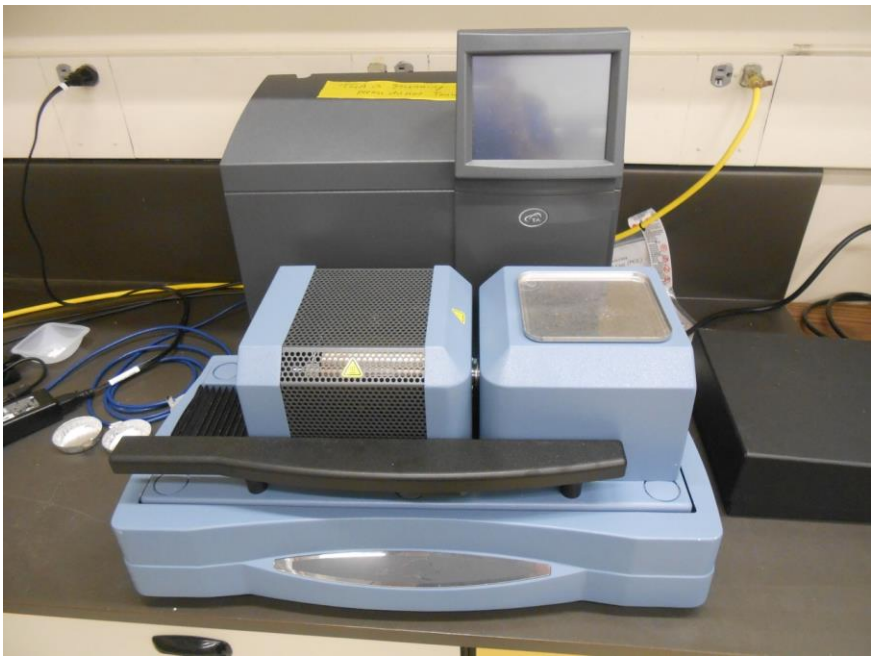

Figure 3.3. Simultaneous thermal analyzer

3.1.4 Autotitrator

Salt samples for titration were taken from the crucibles using a borosilicate tube. It was inserted through an alumina lid placed above the salt and then into the molten salt with one end of the tube sealed with a finger. Collected samples were put into glass bottles, marked and transferred out of a glovebox for titration. Titration was used to measure oxide ion concentration in the salt, as the following reaction should occur when the salt is placed into water.

$$O^{2-} + H_2O \leftrightarrow 2OH^- \qquad (3.1)$$

The OH^- ions generated via this reaction would be automatically titrated with HCl using an SI Analytics TitroLine 7000 autotitrator (see Figure 3.4). A complication to this measurement is that nitrite ions are also expected to generate OH^- ions in aqueous solution according to the following reaction.

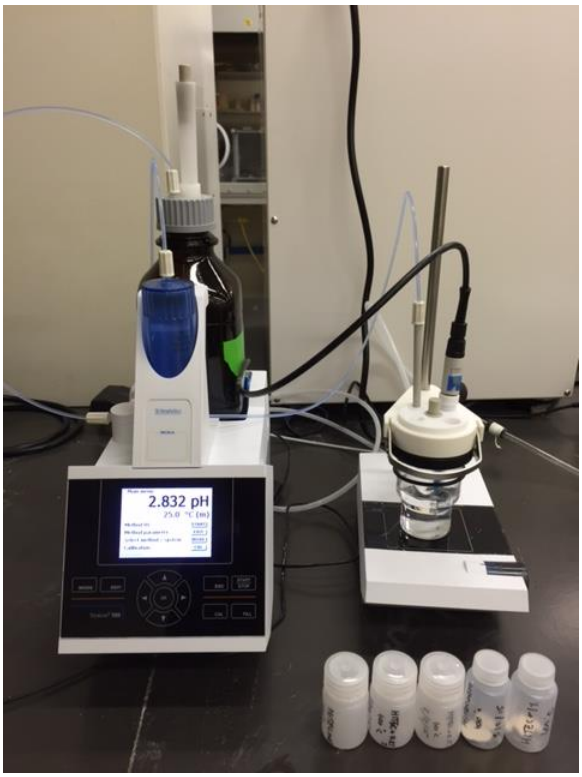

Figure 3.4. Titroline 7000 autotitrator

$$NO^{2-} + H_2O \leftrightarrow OH^- + HNO_2 \quad (3.2)$$

Salt samples with mass of about 0.2 g were dropped into 50 mL of nanopure deionized water and 0.1M HCl at pH of 3.0. As soon as salt sample dissolves, the pH of the solution starts increasing and autotitrator adds a necessary volume of acid to decrease the pH back to 3.0. The final volume of acid consumed was used to calculate the amount of OH^- formed when nitrites and oxides dissolve in DI water.

3.2 Electrochemical Setup

The classic three-electrode electrochemical cell was used for linear sweep voltammetry, square wave voltammetry and cyclic voltammetry experiments. Figure 3.5 shows the electrodes configured within the electrochemical cell.

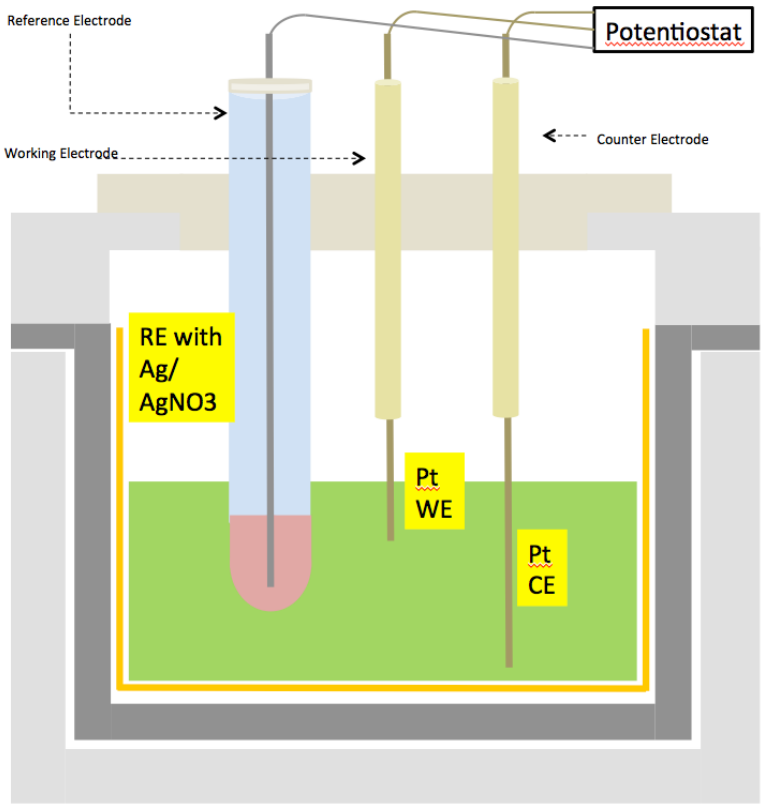

Figure 3.5. General electrochemical setup used

3.2.1. University of Utah Design

Platinum wire from Alfa Aesar (0.5 mm, annealed, 99.95% metal basis) was used both as a working and a counter electrode. The length of the working electrode immersed in the salt was kept constant at 1.25 in., and the length of the counter electrode was selected to be over ten times the length of the working electrode. Platinum wire was coiled to minimize the vertical length of the counter electrode. In earlier experiments, a 2-mm tungsten rod was used as a counter electrode, but it was apparent that tungsten metal dissolved in the nitrate salt, as the electrode decreased in diameter by 30%.

Reference electrodes were made by inserting the silver wire into a mullite tube filled with 2 g of Solar Salt mixed with $AgNO_3$ (10% wt). Earlier experiments used a Pyrex

glass NMR tube. But increasing the temperature led to frequent cracking of the glass tubes due to thermal shock. A thin-walled mullite tube was then used as a substitute, as it was found to be porous enough to allow the ionic migration to occur that is required of the reference electrode. Reference electrode has to be frequently replaced when working with molten nitrates at high temperatures. After multiple uses, the composition of salt and $AgNO_3$ changes significantly and the electrode is not suitable for further experiments. It was also observed that after multiple experiments with molten nitrates at temperatures up to 600 ^{o}C, the outer diameter of mullite tube decreased by 10% as seen in Figure 3.6.

Temperature readings were taken periodically by inserting a thermocouple in one of the ports on top of the alumina lid. Continuous monitoring of temperature was impossible due to the reaction of salt with the thermocouple. The fully assembled University of Utah probe is shown in Figure 3.7

3.2.2 University of Wisconsin Design

The prototype of the probe was built for the existing testing system at the University of Wisconsin. As seen in Figure 3.8, the setup resembles the previous laboratory design. It was decided to replace the expensive platinum wire with 0.25 in. titanium rods with 2 in. of platinum coating. The electrodes were placed in 0.375 in. OD alumina tube, then secured and sealed with o-rings inside of the Swagelok Ultra-Torr fittings. This was done to isolate the rods from the stainless steel flange and to avoid shorts.

Swagelock Ultra-Torr fittings were welded to the 2.75 in diameter CF flange at the University of Utah machine shop. Mullite was chosen as a material for the reference electrode as a sturdier alternative to Pyrex. It was critical to avoid cracks and further

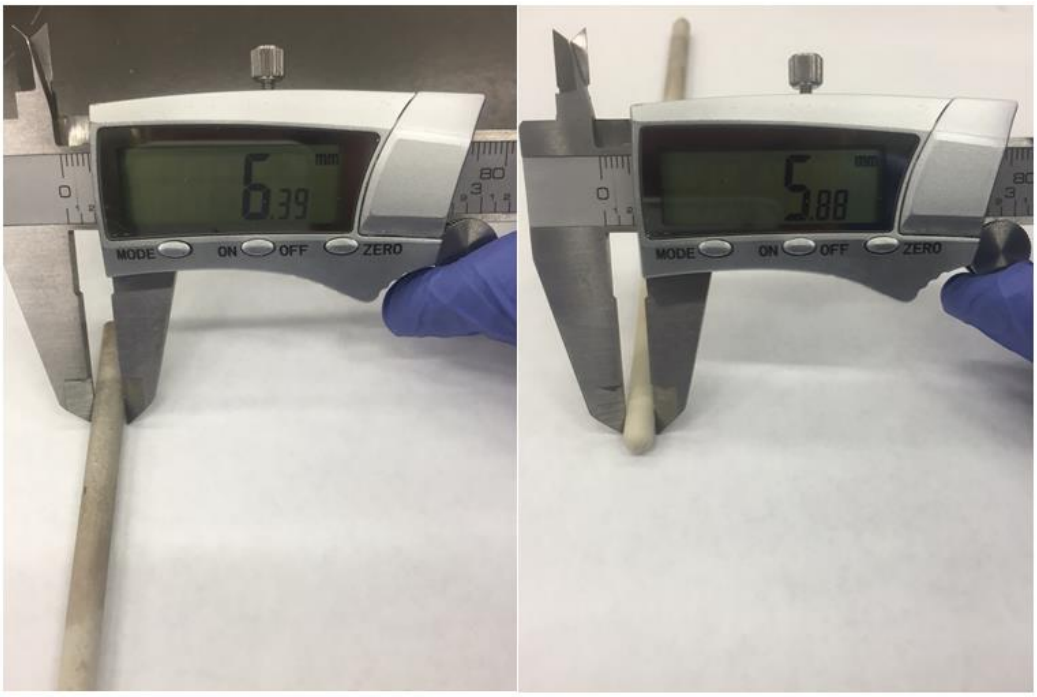

Figure 3.6. Changes in the size of mullite tube after multiple experiments

Figure 3.7. Fully assembled University of Utah probe

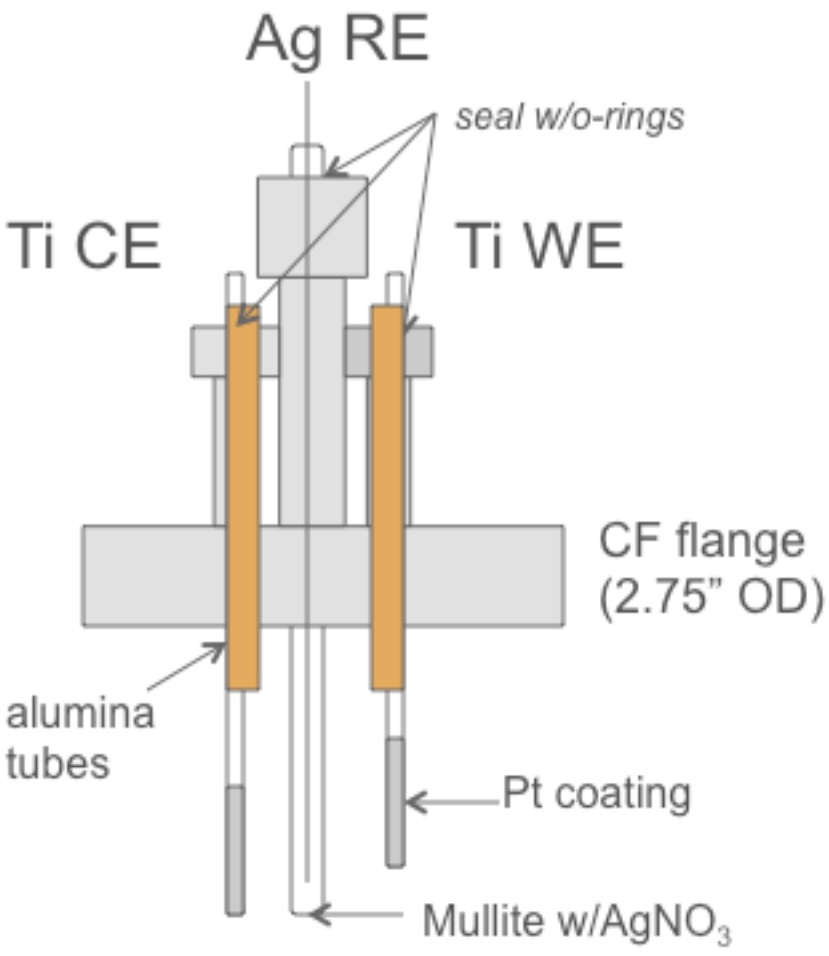

Figure 3.8. Schematic setup of UW probe

contamination of large batches of salt used in the UW system. Figure 3.9 shows the assembled probe before it was delivered to UW.

3.3 Electrochemical Procedures

3.3.1 University of Utah

Solar Salt and HITEC salt were used as received from Abengoa. Solar Salt was prepared in the lab at the University of Wisconsin at Madison by mixing sodium nitrate (refined grade, 99.8%) and potassium nitrate (refined grade, 99.6%) in the ratio of 60% to 40% by weight. Similarly, HITEC was used as received. It was prepared by mixing sodium nitrate, sodium nitrite, and potassium nitrite in the ratio of 7:40:53 percent by weight. All salt came in large chunks and had to be ground up using a regular coffee grinder to make experimental work easier.

For each voltammetry experiment, about 70 g of HITEC or Solar Salt was placed in a 90 mL alumina crucible. Various concentrations of Na_2O (0-1%) were added to simulate the presence of oxide ions. The alumina crucible was then placed into the Kerr Furnace that gradually heated salt to 250^{o}C. It was then heated to a desired temperature at a maximum rate. Measurements were normally taken at least 12 h after the start of the experiment.

The reference electrode (RE) was placed in raw salt and was gradually heated inside of the system to prevent the cracking of mullite due to thermal shock. The working (WE) and counter electrodes (CE) were inserted later when the salt reached the desired temperature. The WE was lightly polished before every experiment. Platinum wire was placed inside of a small alumina tube (1/8 in OD, 1/16 in ID), serving as a sheath. The

Figure 3.9. Assembled UW probe

length of exposed wire was measured with the ruler and kept constant during the experiment.

Experiments were performed both in glove box and in the fume hood. To collect data, the potentiostat was connected to the electrodes, powered up, and connected to a PC. All tests were performed using Nova 1.11, electrochemistry software from Metrohm Autolab. When working in the glove box, the leads from potentiostat were connected to electrodes using electrical feedthroughs in the back of the glove box (5-way binding posts from

Innovative Technologies).

3.3.2 University of Wisconsin

The research group at the University of Wisconsin-Madison worked with HITEC and Solar Salt using a much larger scale furnace and test cell. About 5 kg of salt was loaded into a large alumina liner inside of the custom made insulated furnace that was equipped with 12 thermocouples, several gas sensors, and an FTIR spectrometer, as seen in Figure 3.10. University of Wisconsin's research was focused on analyzing the behavior of the salt by observing changes in its vapor and the cover gas. The probe developed at the University of Utah served as the only tool to analyze the behavior of the molten salt itself. Next, salt samples were sent to the University of Utah to perform titrations due to the lack of equipment in the lab in UW.

The salt was slowly melted overnight, and then the fabricated probe was inserted in the system. The reference electrode was gradually (about 1 cm every 5 min) lowered into the furnace to avoid thermal shock, cracks, and contamination of the system with $AgNO_3$. Identical potentiostat and software package was used at the University of Wisconsin-Madison. All experiments were conducted in regular atmosphere without addition of Na_2O. After taking measurements for over 48 h the salt was disposed; the crucible was washed and prepared for the next experiment.

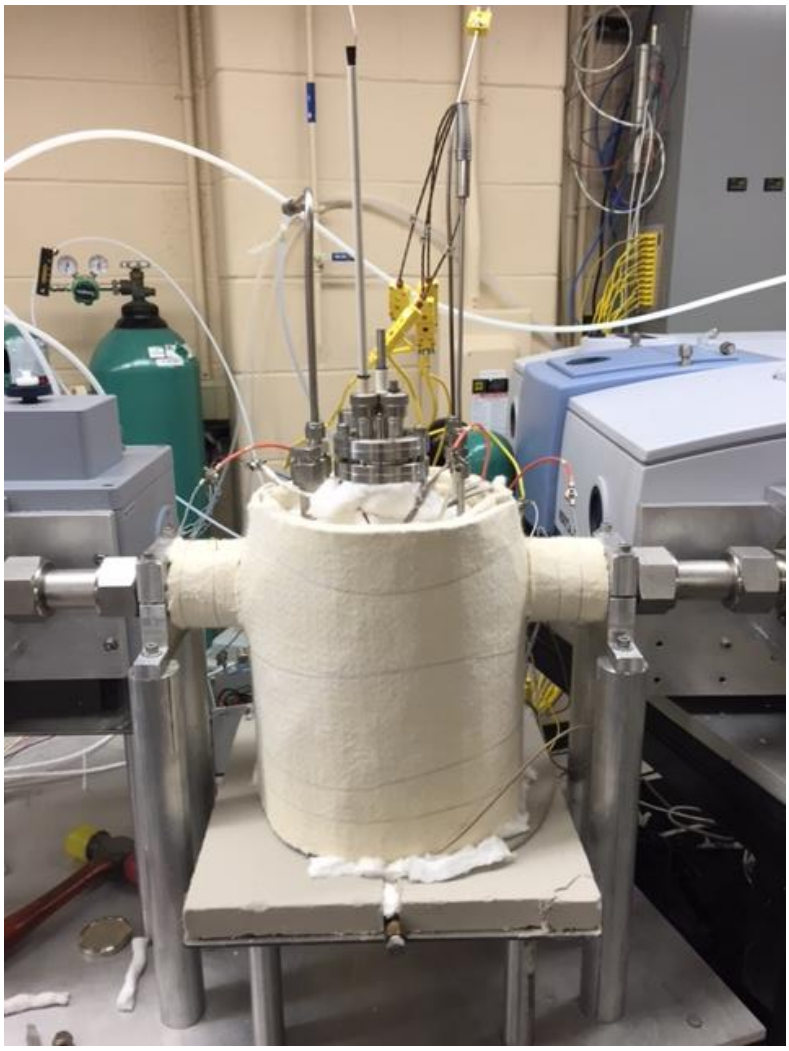

Figure 3.10. Experimental setup at the University of Wisconsin

3.4 Electrochemical Methods

3.4.1. Cyclic Voltammetry and Linear Sweep Voltammetry

Cyclic voltammetry is an electrochemical technique that is used to measure the current developed with changing voltage in an electrochemical cell. The CV is developed by changing the potential of the working electrode and measuring the current. While CV is a great technique, it has several limitations like low resolution and detection limits. It is still, however, a useful tool in determining multiple properties of the system and then choosing a more efficient electrochemical method. CV provides help with identification of cathodic and anodic peaks, potential window, and peaks of interest.

In this study, first CV tests were always performed with pure salt to determine the baseline. After connecting all 3 electrodes to the potentiostat, CV parameters, like start and stop potentials, upper and lower vertexes, scan rate, and the number of cycles, were set in Nova 1.11. Next, identical test with same parameters was conducted with pure salt and 0.5%-1% of Na_2O. Both CV plots were then compared to find the peaks of interest. Linear sweep voltammetry is an electrochemical technique similar to CV. In LSV, the potential of WE is varied linearly in one direction and is not cycled back. Hence, after the peak of interest was identified, LSV procedure was used to obtain the peak current. All parameters were left identical to CV procedure, with the exception of the start and stop potentials.

The following settings were used for the CV procedure:

- Start potential: 0 V
- Stop potential: 0 V
- Upper vertex potential: 0.3 V

- Lower vertex potential: -2.0 V
- Scan rate: 0.15 V/s
- Number of cycles: 3

The following settings were used for LSV procedure:

- Start potential: -1.5 V
- Stop potential: -0.9 V
- Scan rate: 0.15 V/s

3.4.3. Square Wave Voltammetry

Square wave voltammetry (SWV) is a relatively simple electrochemical measurement method. As with CV and LSV, three electrodes (working, counter, and reference) are immersed into the electrolyte liquid (molten salt in this case). The electrical potential of the working electrode relative to the reference electrode is varied according to a specified pulse-like pattern. In SWV, the electric current response is recorded twice, at the end of the forward potential pulse and at the end of the reverse potential pulse. Because of these properties, SWV is used in various applications; it is fast and highly sensitive [33].

In some cases, the peaks observed in SWV are superimposed on larger peaks. To obtain a meaningful value of peak current, it is important to apply baseline correction to SWV plots. In Nova 1.11 this is a built-in function the peaks are corrected according to the moving average.

The following settings were used for SWV:

- Initial potential: -1.2 V
- End potential: 0.6 V

- Step potential: 0.005 V
- Amplitude: 0.02 V
- Frequency: 25 Hz
- Scan rate: 0.125 V/s

CHAPTER 4

RESULTS OF HITEC STUDY

4.1. TGA/DSC Results

Thermogravimetric analysis (TGA) and differential scanning calorimetry (DSC) tests were performed on the HITEC salt samples received from the University of Wisconsin. Since the salt was of relatively low ("refined") grade, it was of critical importance to check the water content, melting point, and decomposition temperature. The salt was ground up inside of the glove box and then transferred to the simultaneous thermal analyzer (STA), which performs both TGA and DSC on a sample at the same time. About 70 mg of HITEC was placed in a small alumina crucible and heated under argon to a temperature of 600°C at a rate of 10°C/min. Figure 4.1 indicates that the melting point is at about 142°C (using on-set temperatures of exothermic peak), which is the value mentioned in multiple publications [13,15,37]. It is a lot more difficult to determine the decomposition temperature with STA. According to Figure 4.2, the mass loss can be observed starting around 500°C. This could be both due to either the vaporization of HITEC or its decomposition. Multiple publications cited the decomposition temperature at 535°C [13,14].

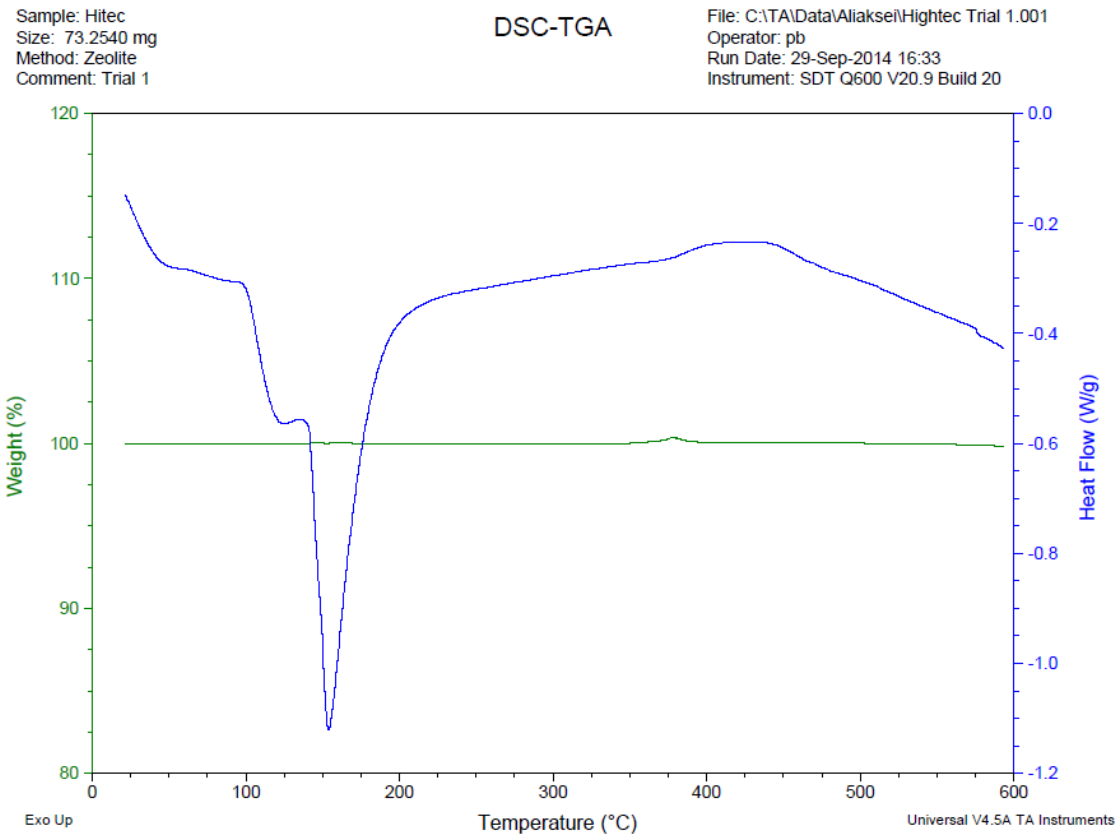

Figure 4.1. TGA/DSC results for HITEC salt

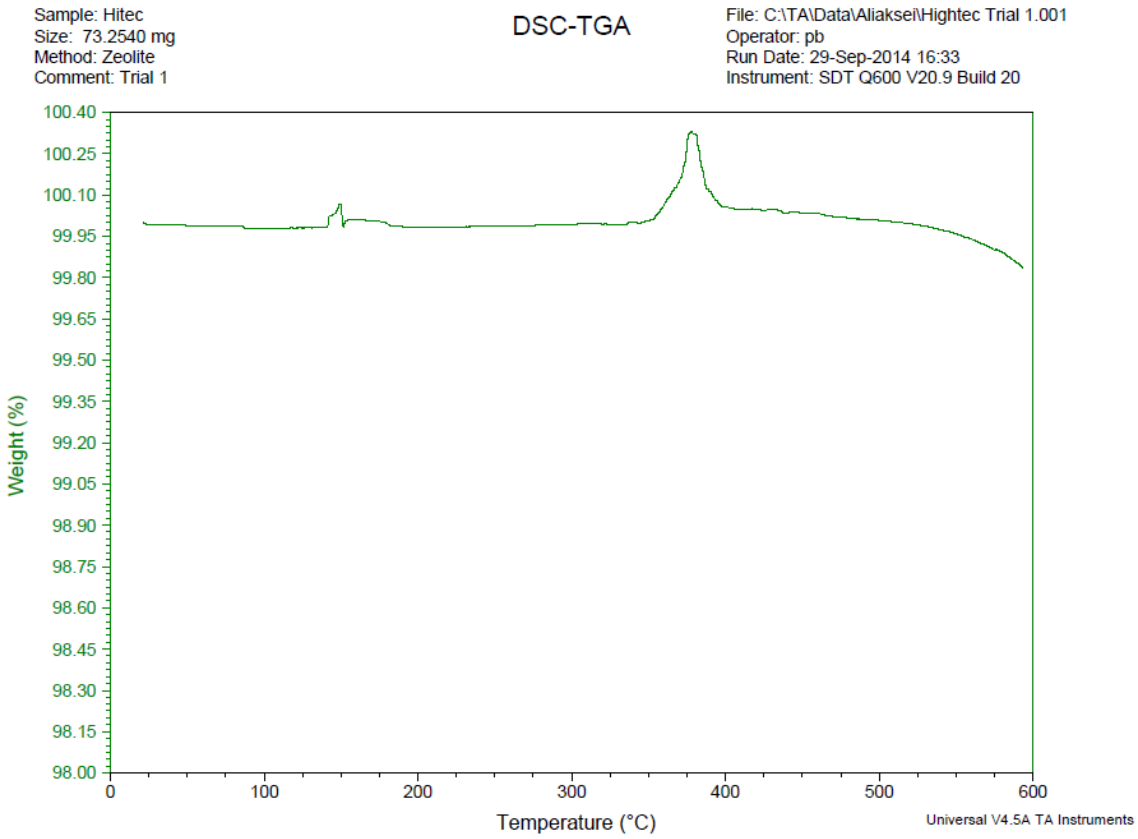

Figure 4.2. TGA results for HITEC salt

4.2 Cyclic Voltammetry Results

CV tests were run with pure HITEC (53% KNO_3, 40% $NaNO_2$, 7% $NaNO_3$) followed by addition of 1% of Na_2O by weight at 360^oC in glove box. The objective was to identify a peak corresponding to O^{2-} ion oxidation to oxygen gas. Cathodic (pointing down) and anodic (pointing up) peaks were identified based on comparison to literature reports [27,33] as shown in Figure 4.3. While CV is not necessarily optimal for concentration measurement, depending on the properties and conditions of the system, it does provide useful information to guide development of the voltammetric method. From Figure 4.3, it can be seen that the potential window is about -2.5V to +0.25 V. At

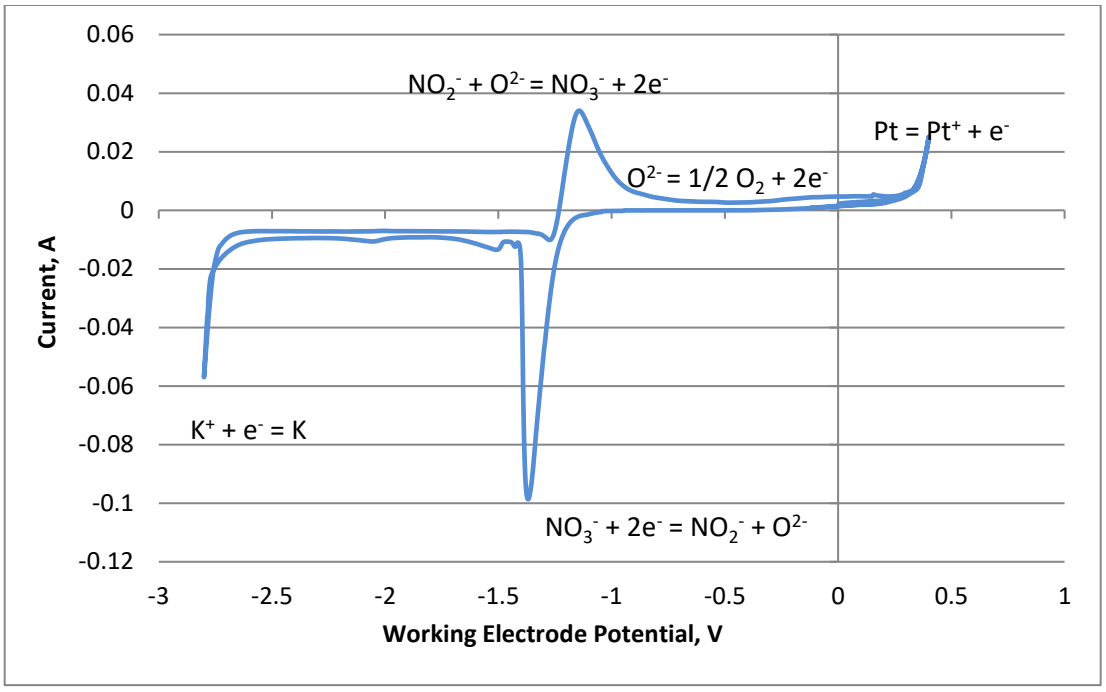

Figure 4.3. Cyclic voltammetry of HITEC salt at 360°C with 1 wt % of Na_2O

higher potentials, the Pt working electrode starts to dissolve. And at lower potentials, the K^+ ions in the salt begin to reduce. Since the salt contains a large concentration of K^+ ions, there is no analytical purpose in reducing these ions. There are two anodic (oxidizing) peaks that could be used to quantify O^{2-} concentration—at about -1.1 V and at about -0.1 V. The former peak is much larger and easily distinguished from the baseline. Since it involves reaction of NO_2^- with O^{2-}, the concentration of both of these anions will contribute to the peak height. HITEC initially has 40 wt % $NaNO_2$ and 7 wt % $NaNO_3$. Both of these concentrations are likely to be very high compared to the range of expected O^{2-} concentrations. Na_2O was added to the salt up to about 1 wt %. Thus, the NO_2^- and NO_3^- concentrations are assumed to be relatively constant so that the peaks really only vary in intensity based on O^{2-} concentration. Still, it was decided to try to avoid the NO_3^- reduction peak so as to keep the NO_3^-/NO_2^- ratio constant.

4.3. Linear Sweep Voltammetry Results

Due to the proximity of the reduction and oxidation peaks, it would be hard to avoid NO_3^- reduction peak and keep the NO_3^-/NO_2^- ratio constant while using CV. However, this can hypothetically be accomplished by scanning in only one direction (negative to positive in this case). Hence, it was determined that linear sweep voltammetry (LSV) is the appropriate electrochemical method for this task.

4.3.1. Scan Rate Experiments

A series of LSV runs using HITEC salt are shown in Figure 4.4. Experiments were performed inside of the glove box at 360°C with addition of 0.75 wt % Na_2O. LSV data was collected for 5 different scan rates ranging from 0.1 to 0.3 V/s. Two peak current values were measured for each scan rate. It is evident from this plot that the results were repeatable at each scan rate.

The peak heights were averaged and plotted versus the square root of the scan rate (see Figure 4.5). The Randles-Sevcik equation (4.1) given below predicts that the peak heights should vary linearly with the square root of the scan rate, and the plot should go through the origin:

$$I_p = 0.4463(nF)^{\frac{3}{2}}\left(\frac{\nu}{RT}\right)^{\frac{1}{2}} CA\sqrt{D} \tag{4.1}$$

where A is electrode area (cm^2), C – concentration (mol/cm^3), D – diffusion coefficient (cm^2/s), F – Farraday Constant (C/mol), I_p – peak current (A), n – number of electrons transferred, R – gas constant (J/K-mol), T – temperature (K), and ν – scan rate (V/s). In this case, there is mixed agreement with the Randles-Sevcik equation. The peak height does vary linearly with square root of scan rate. But the plot does not intersect the origin.

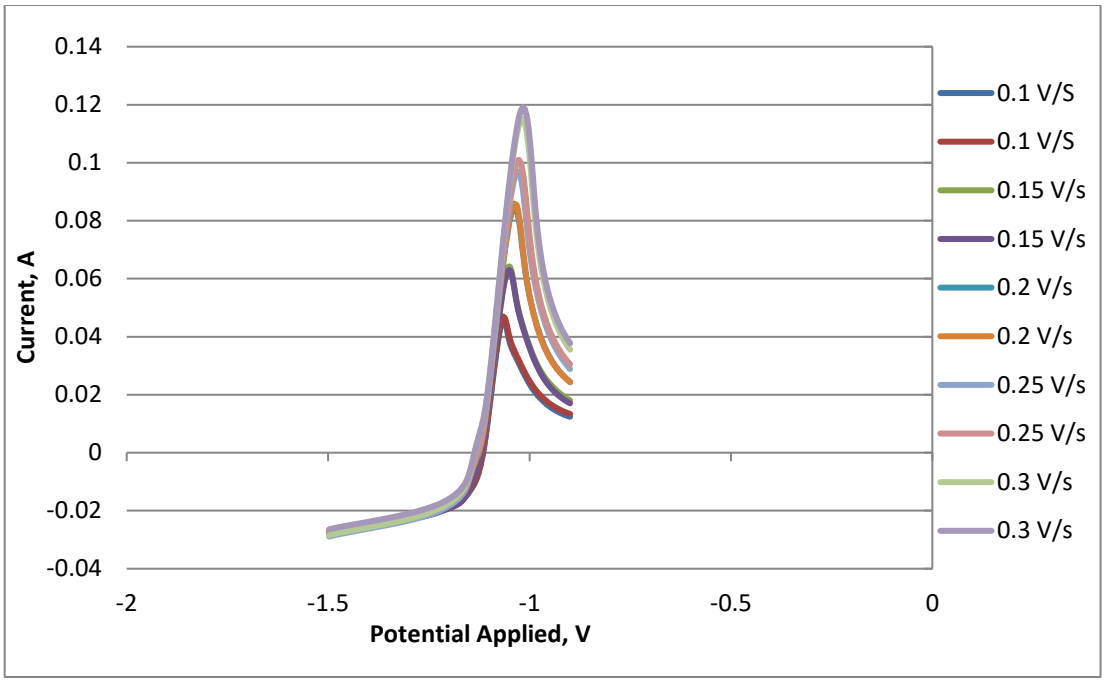

Figure 4.4. Linear sweep voltammetry of HITEC salt at 360°C with 0.75 wt % Na_2O

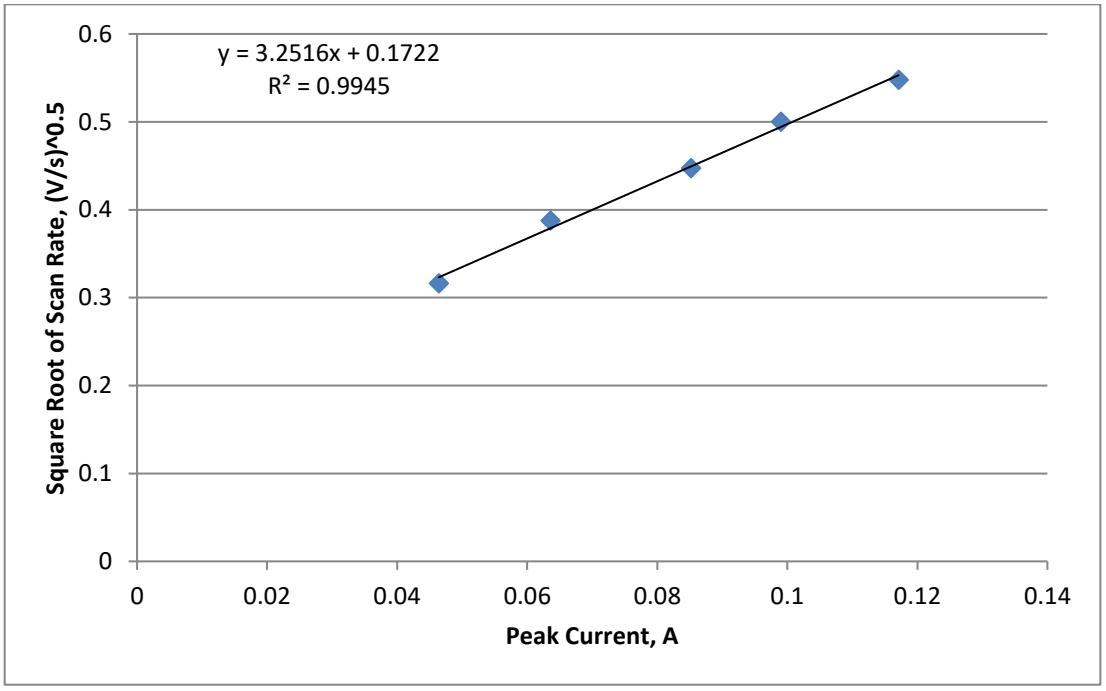

Figure 4.5. Peak current values plotted versus square root of scan rate for HITEC salt with 0.75 wt % Na_2O added at 360°C

Usually, what this means is that the electrochemical reaction is either quasi-reversible or irreversible in the range of scan rates investigated [38]. As the scan rates are reduced, it is likely that the reversible region will be approached. But sometimes it is impractical to run in the reversible region. Note that if it was possible to run in the reversible region that the plot should intersect the origin and the slope could be used to calculate the diffusivity of O^{2-} in the salt. Once D is known, then the Randles-Sevcik equation can be used to calculate concentration in moles/cm^3 based on the slope of the plot shown in Figure 4.5.

4.3.2. Concentration Correlations

Alternatively, it may be possible to measure empirical relationships between concentration and peak height. Even if the Randles-Sevcik equation is not strictly applicable to this system, there still may be a continuous, regular relationship between peak height and concentration with other variables such as scan rate and temperature held constant. A relatively low temperature (T=360^{o}C) calibration curve for HITEC is shown in Figure 4.6. These experiments were performed in a fume hood with air atmosphere. Attempts to measure higher temperature calibration curves were unsuccessful, possibly due to effects described below.

Even before switching the focus to Solar Salt, important insight into the nitrate salts was obtained using HITEC. An important objective of this project is to provide data to facilitate increasing the process temperature. It is, thus, important to know if the peak intensities are also functions of temperature. If the Randles-Sevcik equation can be referred to as a guide even outside of the reversible reaction region, it can be seen that

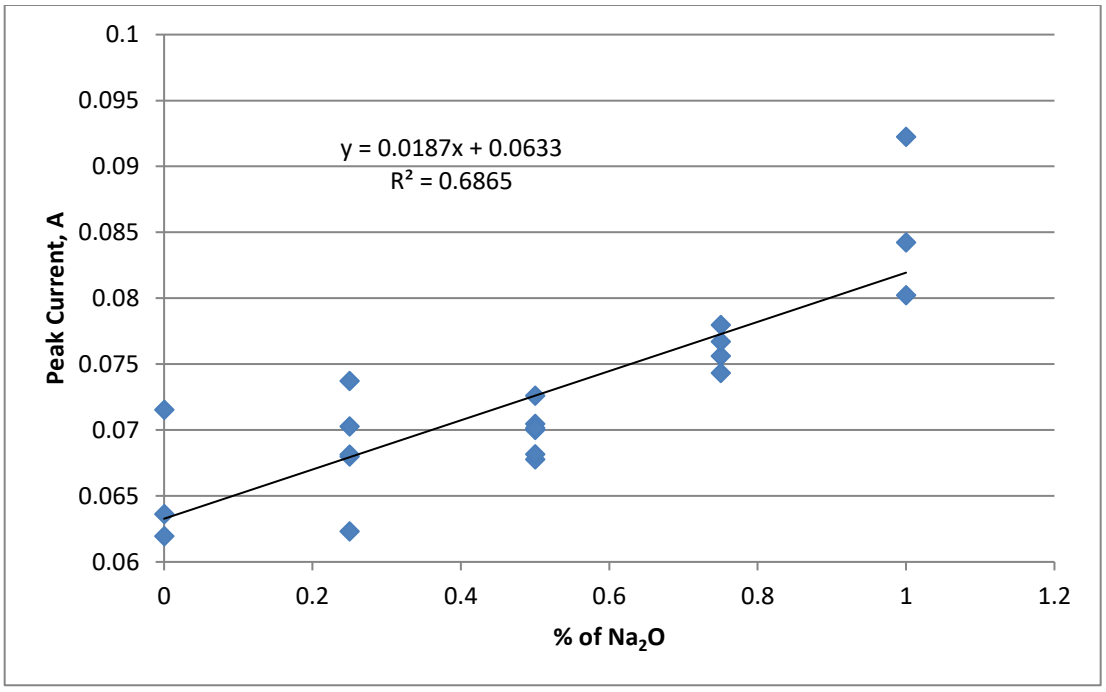

Figure 4.6. Calibration curve for Na_2O concentration in HITEC at 360°C and the WE immersion depth is 2.5 cm (Area = 0.395 cm^2)

increasing the temperature is expected to reduce the peak heights. A series of LSV runs were completed with HITEC salt at temperatures ranging from 360 to 405°C with a Na_2O concentration of 1 wt %, and the results are shown in Figure 4.7. Here it is evident that the peak heights actually increased with increasing temperature. This could be due to concentration dependence of the diffusion coefficient. Or, it could be due to an increase in the O^{2-} concentration caused by degradation of the salt as the temperature rises. The fact that the salt decomposition occurs and leads to an increase in O^{2-} concentration via the following reaction (4.2) [39] in general complicates the task of developing calibration curves for O^{2-} concentration.

$$2NaNO_2 \rightarrow Na_2O + NO + NO_2 \qquad (4.2)$$

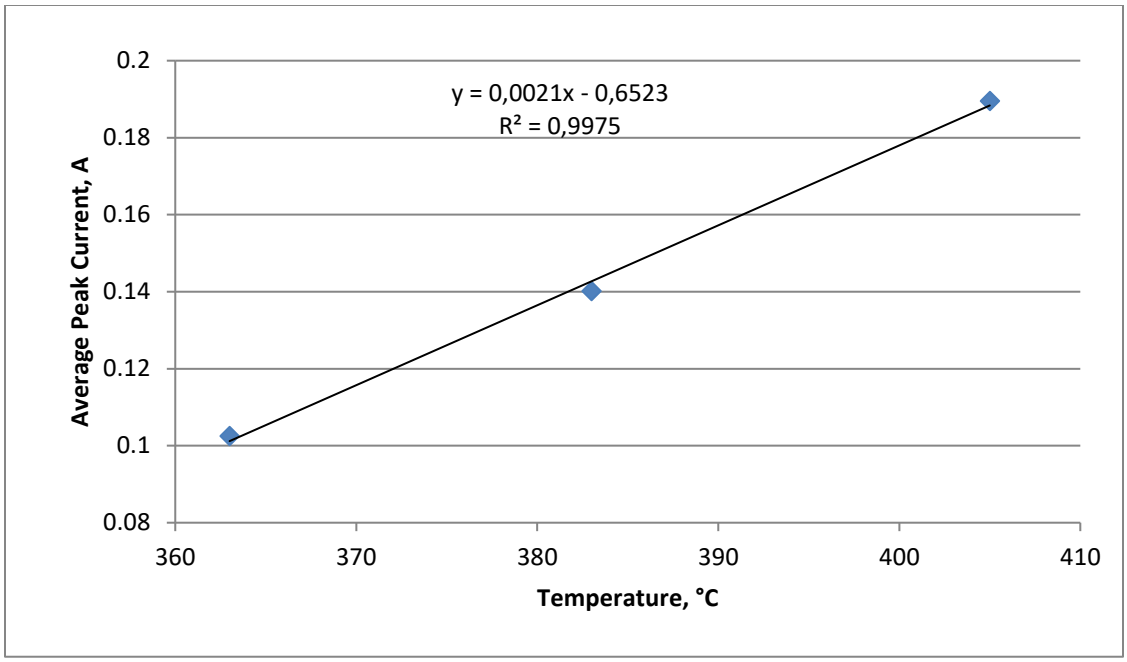

Figure 4.7. Effect of temperature on LSV peak current for HITEC with 1 wt % Na_2O added. Working electrode area = 0.395 cm^2

4.3.3. Time Effects

After running multiple tests with HITEC with 1 wt % of Na_2O at higher temperatures (>450^oC) it was discovered that the salt changes its color to darker yellow, presumably decomposes, and produces inconsistent LSV results. The change in color of the salt is likely caused by the generation of NO_x compounds as per the chemical equation shown above (4.2). If that were the case, it would also affect the LSV peak heights due to generation of O^{2-} ions in the salt. Refer to the series of LSV plots overlaid in Figure 4.8. For this series of measurements, the O^{2-} concentration was in theory zero due to no Na_2O added. These experiments were conducted in the fume hood. With increasing time at constant temperature, the peak height increases. It was initially assumed this was due to conditioning of the salt from off-gas of water or some similar process. But it was likely due to a progressive increase in the concentration of O^{2-} ions in the salt.

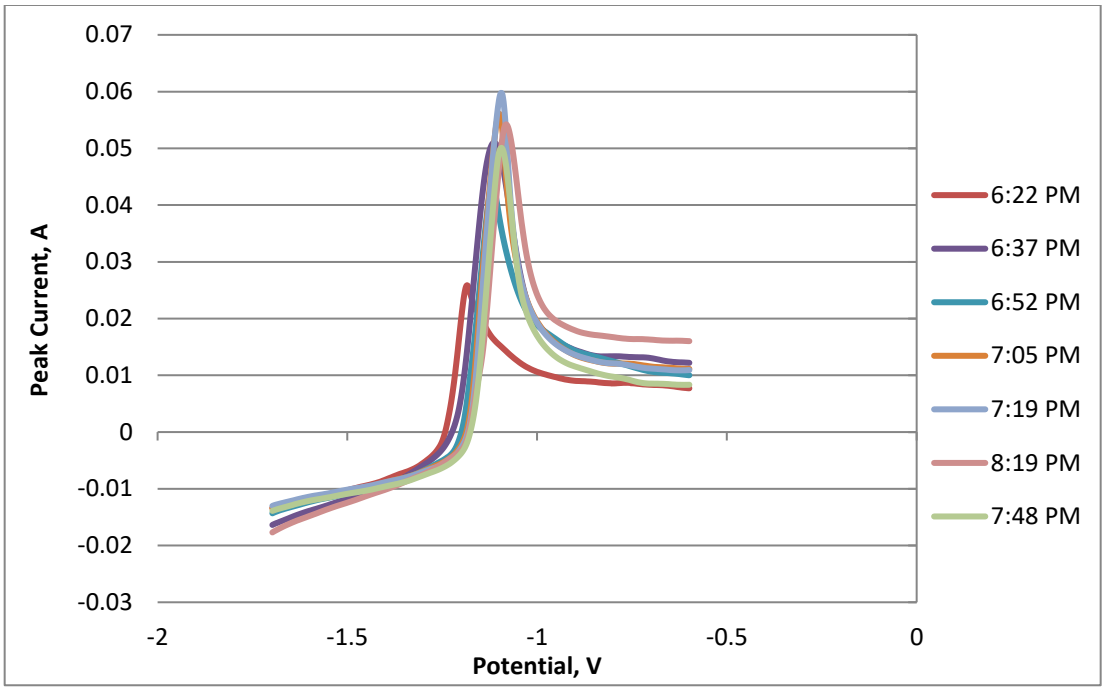

Figure 4.8. Linear sweep voltammetry of pure HITEC salt at 360°C.

The peak heights from Figure 4.8 in addition to those from another run are plotted versus time at temperature (360°C) in Figure 4.9. The results are repeatable and consistent with the conclusion that O^{2-} is actively generated in the salt due to decomposition of the sodium nitrate salt.

Essentially, the in-situ generation of O^{2-} in the HITEC salt makes the voltammetry analysis a matter of trying to hit a moving target. The experimenter can weigh out a specific amount of Na_2O in order to try to establish the O^{2-} concentration. But if more O^{2-} is generated when the salt is heated to the temperature of interest, the calibration curve becomes perturbed in a way that is difficult to quantify. It was originally anticipated that dissolving samples of the salt into water and performing a titration would give us a direct measurement of the O^{2-} concentration. Then a sample taken at the same time as the voltammetry scan could be used to correct the O^{2-} concentration. However, it

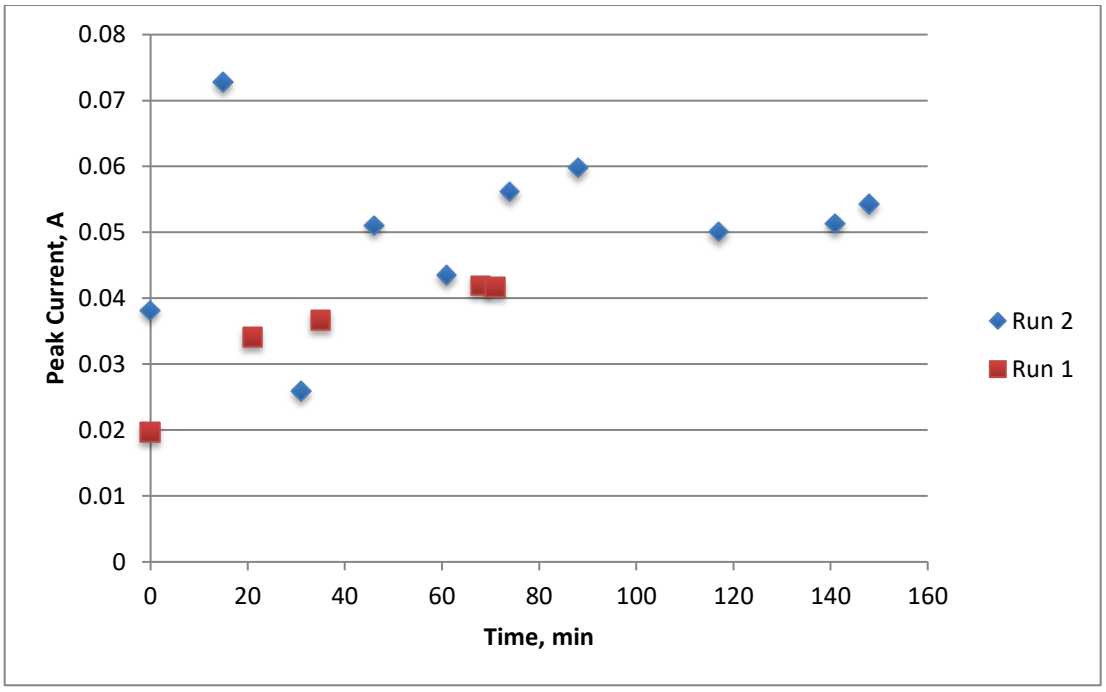

Figure 4.9. heights measured using LSV with pure HITEC at 360ºC Effect of time on the peak

was found that HITEC salt without any added Na_2O resulted in a positive amount of titration. It was determined that is this due to NO^{2-} reacting with water to form HNO_2 and OH-. Ultimately, this makes the measurement of O^{2-} in HITEC via wet chemical analysis to be very difficult. Unless a chemical method can be applied to differentiate between O^{2-} and NO^{2-} in the salt, then the actual O^{2-} concentration will always be unknown. And calibration curves cannot be reliably measured unless it is assumed that the temperature is low enough to minimize the amount of O^{2-} generated during the measurement.

CHAPTER 5

RESULTS OF SOLAR SALT STUDY

Solar Salt is another nitrate salt mixture that is of high interest for application to CSP systems. Its nominal composition is 60% $NaNO_3$ and 40% KNO_3. Its nominal melting point is 222°C.

5.1. TGA/DSC Results

A sample of Solar Salt of relatively low ("refined") grade was received from the University of Wisconsin. Water content, melting point, and decomposition temperature were measured with TGA/DSC. Solar Salt was ground up inside of the glove box and about 32 mg were placed in a small alumina crucible and then transferred to the STA. The salt was heated at 10.00°C/min to 120.00°C, then at 1.00°C/min to 180.00°C, and at 5.00°C/min to 700.00°C. Results of TGA/DSC with Solar Salt shown in Figure 5.1 indicate that it melts at about 220°C, which is very close to previous cited values [13,19,37].

Figure 5.2 indicates that Solar Salt delivered from the University of Wisconsin had a water content of about 3% by weight according to TGA results. Since most of the water is removed at about 360°C, it was decided that there is no need to dry the salt before experiments. Furthermore, experiments were run for over 12 h, which allowed almost

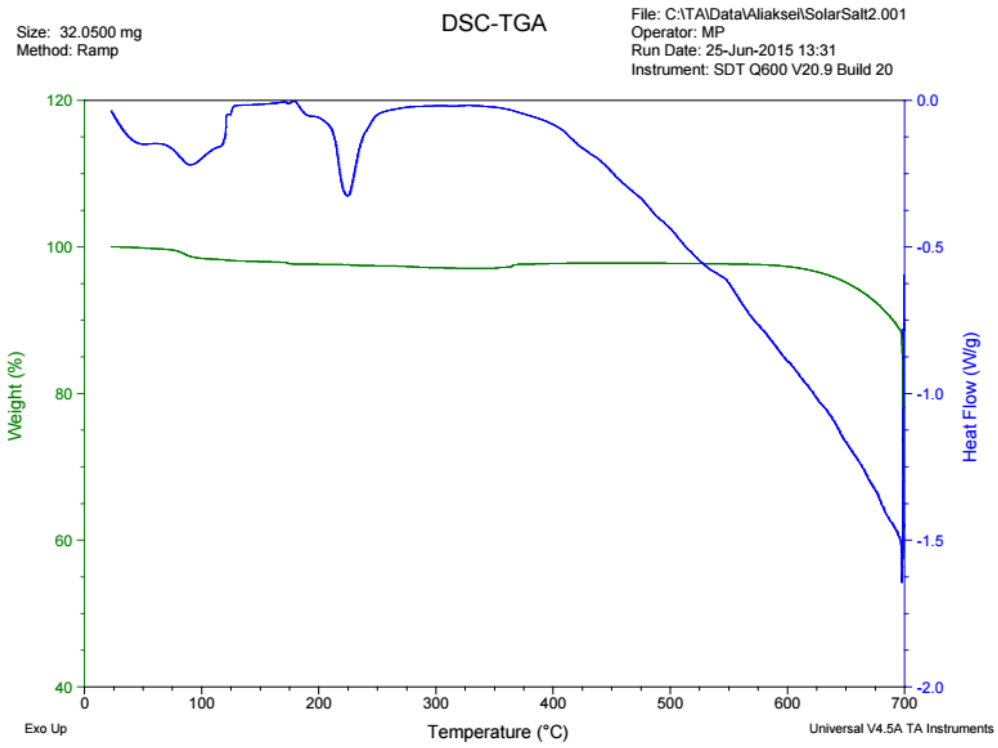

Figure 5.1. TGA/DSC analysis of Solar Salt

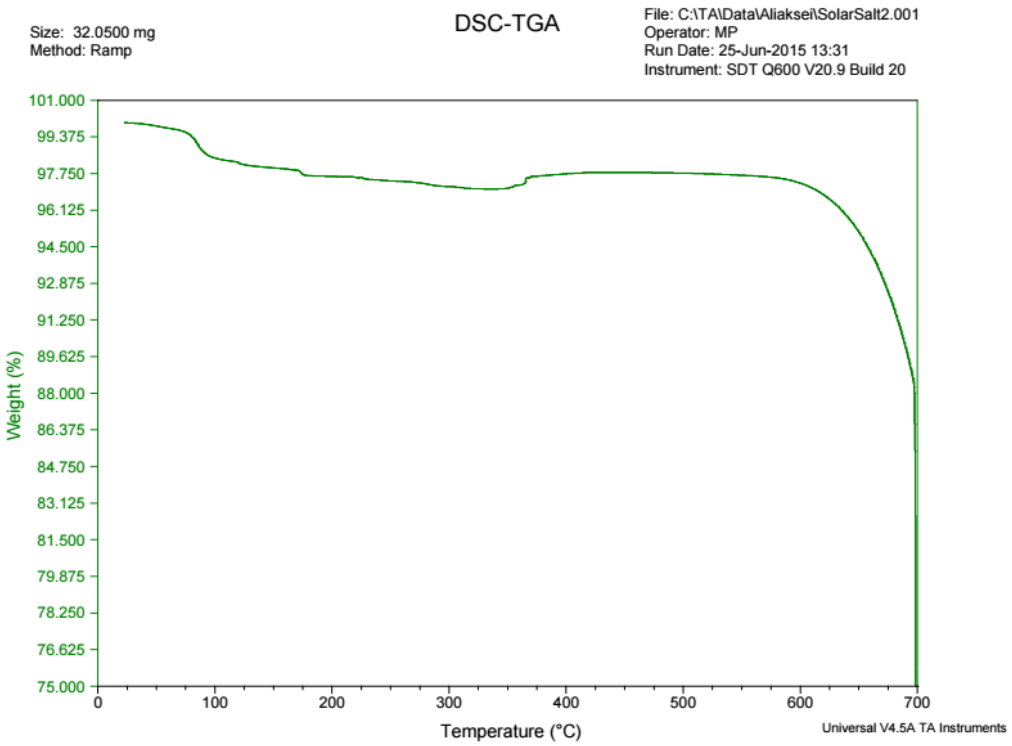

Figure 5.2. TGA analysis of Solar Salt

complete removal of water. This figure also shows how fast the decomposition occurs at higher temperatures. Again, it is hard to estimate the exact decomposition temperature due to evaporation of the salt. However, significant mass loss is observed at about 550°C.

5.2. Cyclic Voltammetry Results

First, to determine the peaks of interest, simple CV tests were performed with pure Solar Salt followed by tests with Solar Salt and 0.5% of Na_2O by weight (see Figure 5.3). The absence of NO^{2-} ions in the salt, unfortunately, takes away the major peak that was used for HITEC analysis. Instead, we had to look for the O^{2-} oxidation peak, which was known to be very small from the testing with HITEC. For Solar Salt, the introduction of Na_2O created a broad peak at around 0.1-0.2 V (see Figure 5.4). It was, thus, deduced that

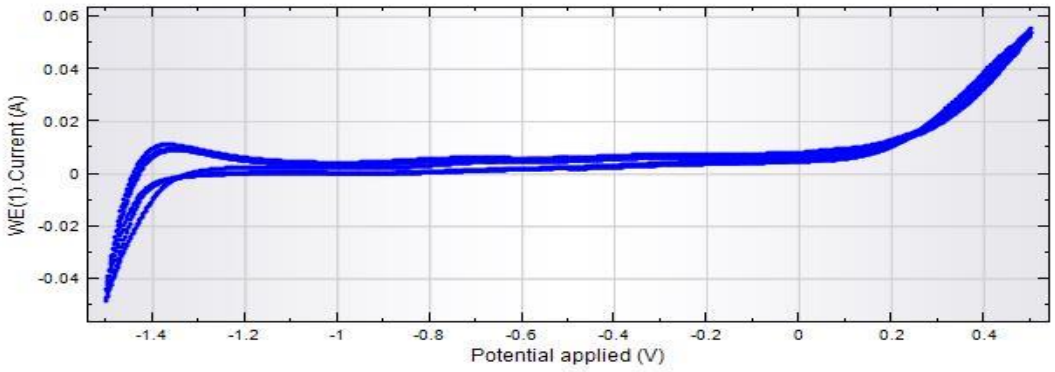

Figure 5.3. CV of pure Solar Salt at 415°C

this peak's size could be correlated to the O^{2-} concentration.

5.3. Square Wave Voltammetry Results

Square wave voltammetry (SWV) is often applied to measurement of dilute species when CV is not adequately sensitive, as shown in the case of Solar Salt in Figure 5.4. This method was thus applied to Solar Salt. An example of a raw SWV result is shown in Figure 5.5. The peak of interest based on the CV analysis is at about 0.1 V.

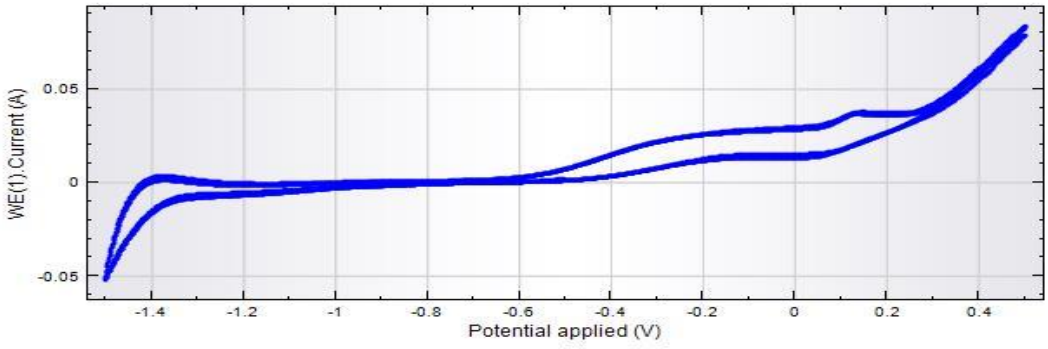

Figure 5.4. CV of Solar Salt and 0.5 wt % of Na_2O at 415°C

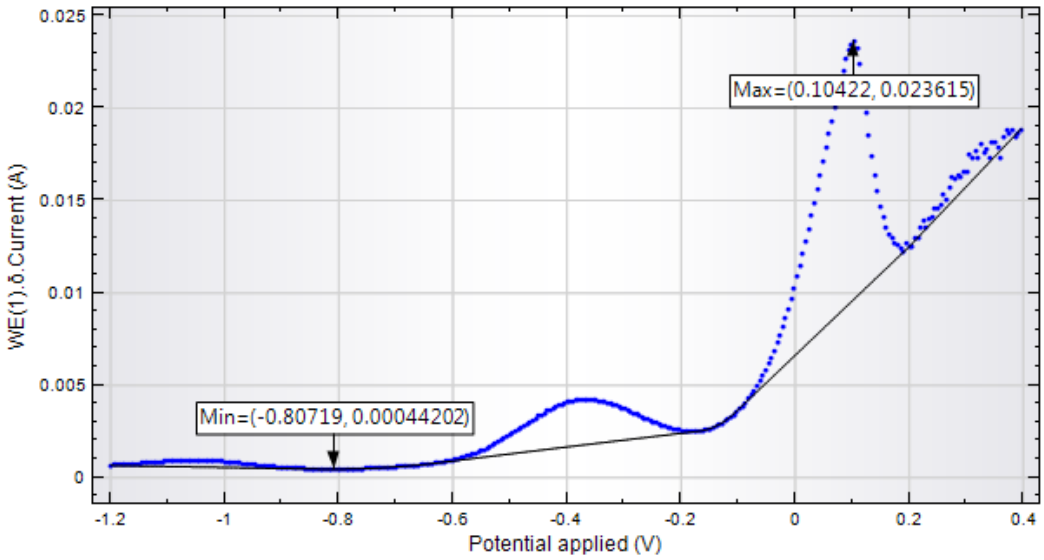

Figure 5.5. SWV of Solar Salt with 0.5 wt % added Na_2O at 415°C

5.3.1. Baseline Correction

Since the peak appears to be overlapped onto a larger peak, it is necessary to perform a background subtraction. This can be performed directly within the Nova software. The result after moving average baseline correction is shown in Figure 5.6. To verify that this peak is due to O^{2-} ions, SWV was run for pure Solar Salt. The result is shown in Figure 5.7. It is clear that there is no peak at 0.1 V. Thus, we adopted the method of SWV for Solar Salt and focused our analyses on the peak at about 0.1 V.

5.3.2. Decomposition of Solar Salt

According to several sources [16,17], decomposition of Solar Salt occurs via the following reactions:

$$NaNO_3 \leftrightarrow NaNO_2 + \frac{1}{2}O_2 \tag{5.1}$$

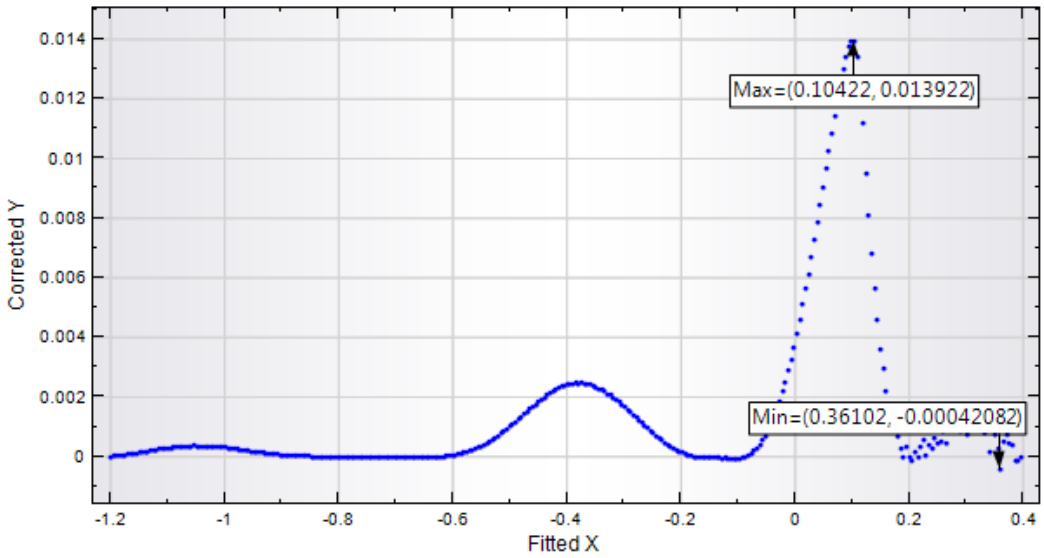

Figure 5.6. SWV of Solar Salt with 0.5 wt % added Na_2O at 415°C after baseline correction

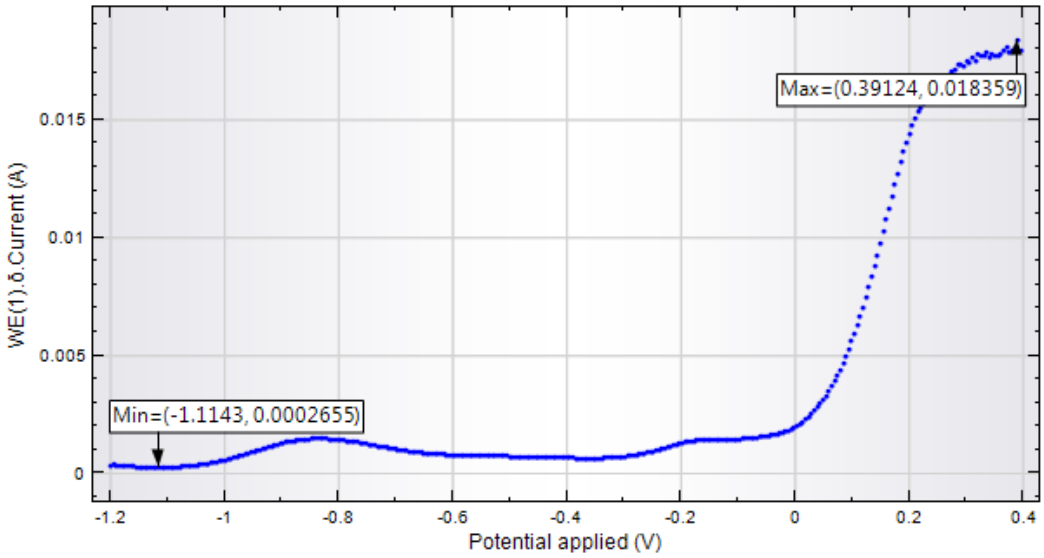

Figure 5.7. SWV of pure Solar Salt at 415°C

$$2NaNO_3 \leftrightarrow Na_2O + \frac{5}{2}O_2 + N_2 \quad (5.2)$$

The nitrites produced via 5.2 decompose further via this reaction [39]:

$$2NaNO_2 \rightarrow Na_2O + NO + NO_2 \quad (5.3)$$

What is unknown is what temperature is required to drive the second reaction and can it be shifted to the left by introducing NO_x into the cover gas. The O^{2-} generated from this reaction can be detected using SWV as previously discussed. But if the calibration curve cannot be measured at a temperature below which decomposition occurs, then the same problem exists as with HITEC.

To initially check the effect of temperature, square wave voltammetry (SWV) tests were performed with pure Solar Salt in the fume hood. Temperature was gradually raised for each run, and the SWV scans were performed. As shown in Figure 5.8, both the peak at -1 V and the peak at about 0.1 V increase as the salt temperature is increased from 418 to 560^{o}C. The peak at -1 V is likely to be due to the reaction of NO^{2-} with O^{2-}. At lower temperatures, this peak was not even observed. Thus, the $NaNO_3$ decomposition reaction must start to occur at these temperatures, generate some $NaNO_2$, which then decomposes to for O^{2-}. Both peaks were observed to be significantly affected by the temperature.

While performing this experiment, it was discovered that salt vapors react with a graphite liner of Kerr furnace in air atmosphere. As seen in Figure 5.9, the graphite crucible was damaged, and the salt was contaminated. It was decided to run the next set of high temperature tests in an inert argon atmosphere inside of the glovebox. It was determined that at temperatures higher than 580^{o}C the salt becomes very unstable even in argon and starts decomposing rapidly, releasing oxygen in glovebox. This oxygen was detected using the glove box oxygen sensor. The glove box has an alarm system that

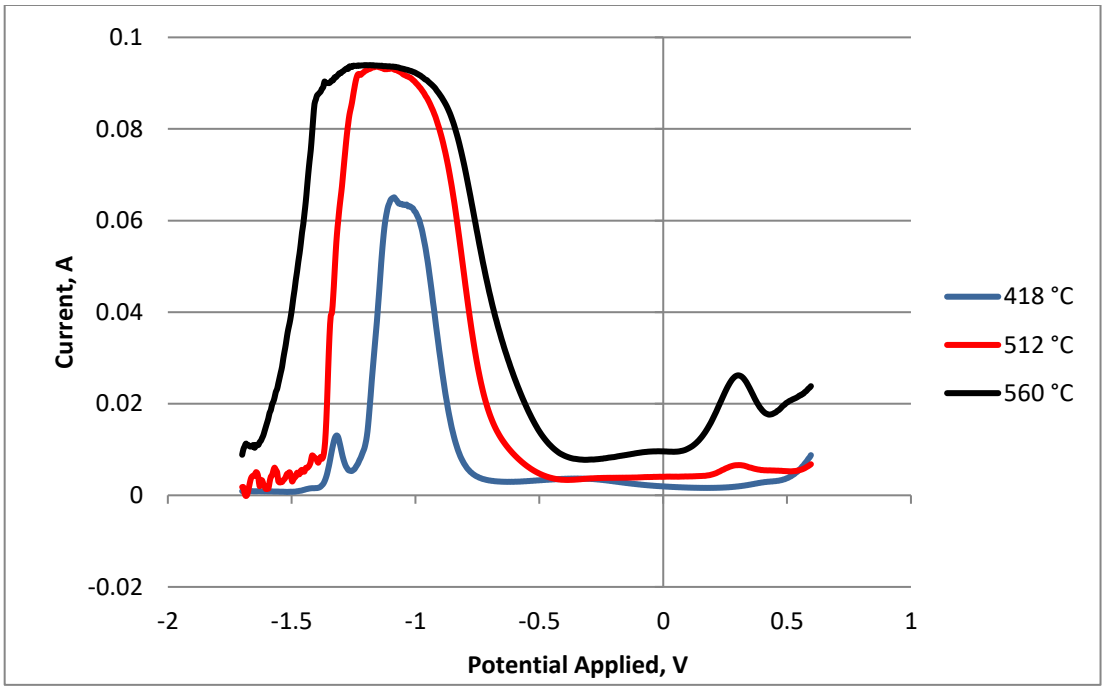

Figure 5.8. Effect of temperature on SWV of pure Solar Salt

Figure 5.9. Damaged graphite liner after high temperature experiments in the fume hood

alerts the user when the oxygen concentration reaches 100 ppm. This set point was exceeded multiple times during the series of experiment with values reaching up to 450 ppm.

5.3.3. Concentration Correlations

Using the SWV method, calibration curves were measured for Na_2O concentration versus peak current at three temperatures – 540 , 560, and 580ºC. All of the experimental data collected is plotted in Figure 5.10. Averaged values of the peak heights are plotted in Figure 5.11. There is clearly an effect of temperature on the results. This could be due to actual temperature-based effect on the peak current for a given concentration. Or it could be due to the possibility that O^{2-} concentrations are actually increasing as the temperature increased and the x-values of these plots may be inaccurate. This is a very difficult problem to de-convolute and likely contributes to much of the noise shown in these plots.

The calibration curves are of the following form:

$$I_p = (slope) \times [Na_2O\ concentration\ in\ wt\ \%] + (y - intercept)\ Amps \quad (5.4)$$

And the parameters are given in Table 5.1. Note that current is proportional to working electrode area, which is 0.5 cm^2 in this case. If the WE area is changed, the current will scale linearly with area.

5.4. Solar Salt Experiments at the University of Wisconsin

To support the development, construction, and calibration of a voltammetry probe that could be installed in the large scale molten salt pot at the University of Wisconsin,

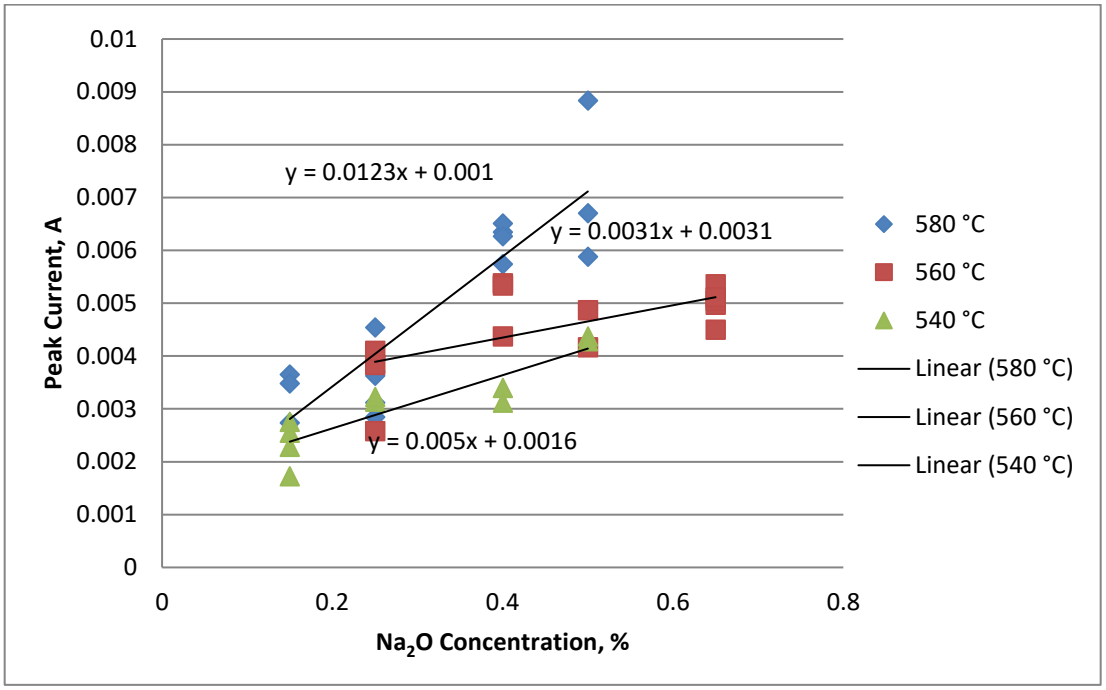

Figure 5.10. Calibration curves for Na_2O concentration in Solar Salt with all data plotted. WE area = 0.505 cm^2

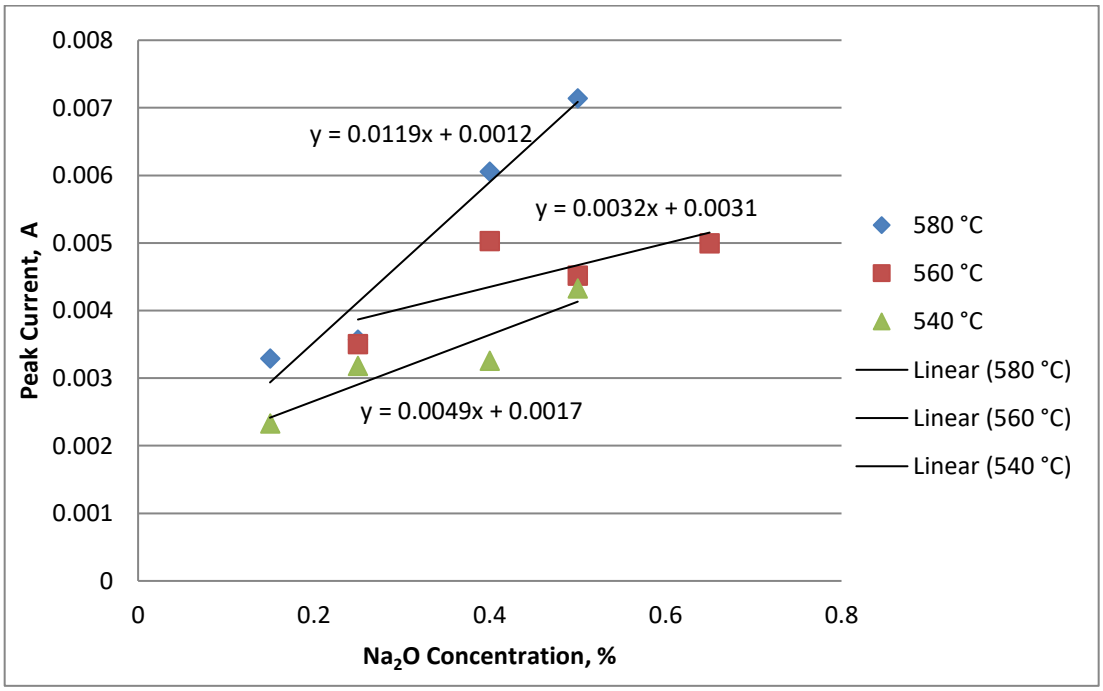

Figure 5.11. Calibration curves for Na_2O concentration in Solar Salt with averaged data plotted. WE area = 0.505 cm^2

Table 5.1. Calibration plot parameters for Na_2O concentration (wt %) versus peak current in Solar Salt. WE area = 0.505 cm^2.

Temperature (°C)	**Slope**	**y-intercept**	**R^2**
540	0.0049	0.0017	0.867
560	0.0032	0.0031	0.579
580	0.0119	0.0012	0.957

SWV based calibration curves were generated in our lab using platinum wire as a working and counter electrode. Figure 5.12 shows the data collected after running the experiments in the fume hood at 415°C.

Next, the new probe was tested using the Pt-coated Ti rods (0.25 in. diameter) and another calibration curve (see Figure 5.13) was created at the same temperature. Due to the small size of Kerr furnace, the placement of electrodes differed from the one at UW. It was also impossible to use the alumina tubes so Teflon tape was used for isolation of electrodes instead. The possible immersion depth of the working electrode was limited and was kept around 1.5 mm. With immersion depth this small it is difficult to estimate the correct area of working electrode.

As soon as the probe was fully assembled and tested, it was delivered to the University of Wisconsin. There, first SWV experiments with pure Solar Salt at 350°C produced a zero current signal. It was later determined that SWV worked well when a large alumina crucible was placed inside of the metallic salt pot. This can be explained by the limited capabilities of Autolab PGSTAT302N. This particular potentiostat model.

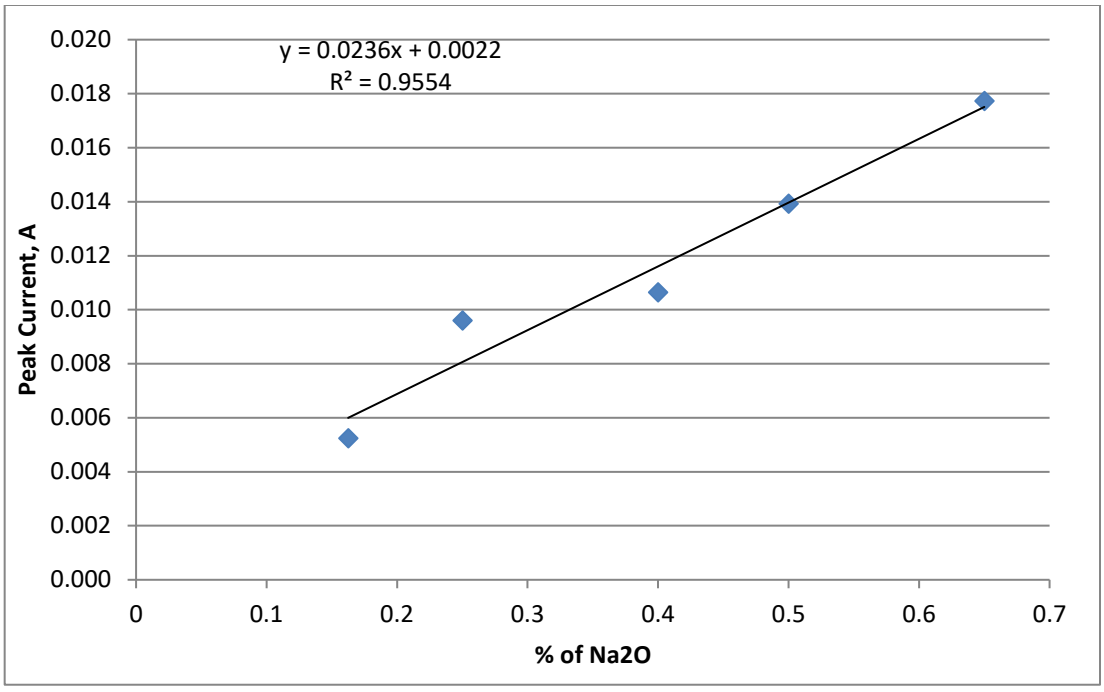

Figure 5.12. Calibration curve for Na_2O concentration in Solar Salt at 415°C (platinum electrode area = 0.395 cm^2)

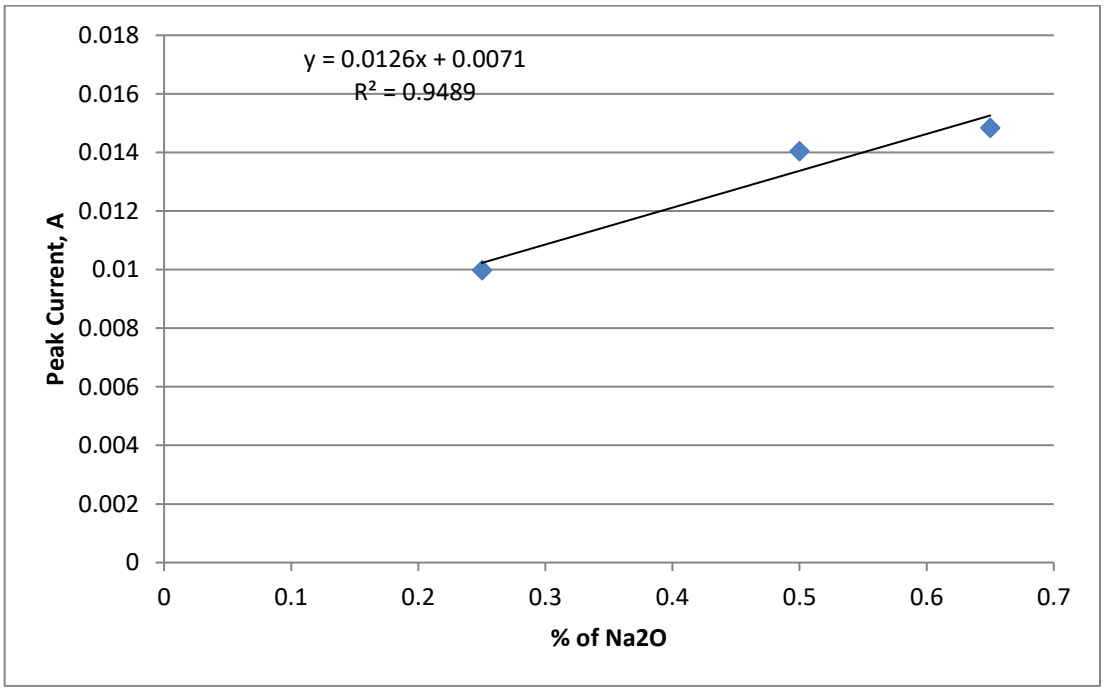

Figure 5.13. Calibration curve for Na_2O concentration in Solar Salt at 415°C (Ti rod electrode area = 0.616 cm^2)

does not work with floating ground systems. As soon as alumina crucible was placed inside of the salt tank, UW research group received their first promising results. Same peaks of interest were observed at 600ºC at the UW, as seen in Figure 5.14. As expected, they occurred at higher temperatures due to the decomposition of nitrates. There was no Na_2O added to the UW system at any point.

As it was mentioned earlier, the research group at the University of Wisconsin was largely focused on the influence of the cover gas on the behavior of the salt. Readings from the probe were recorded and sent to the University of Utah for analysis together with salt samples for titration. Oxygen, nitrogen, and dry air were tested as three main cover gases. The probe performed the best when used with oxygen as a cover gas.

The experiment lasted for one week and the salt temperature was raised every day or every other day, as seen in Table 5.2. One of the technicians performed SWV tests and

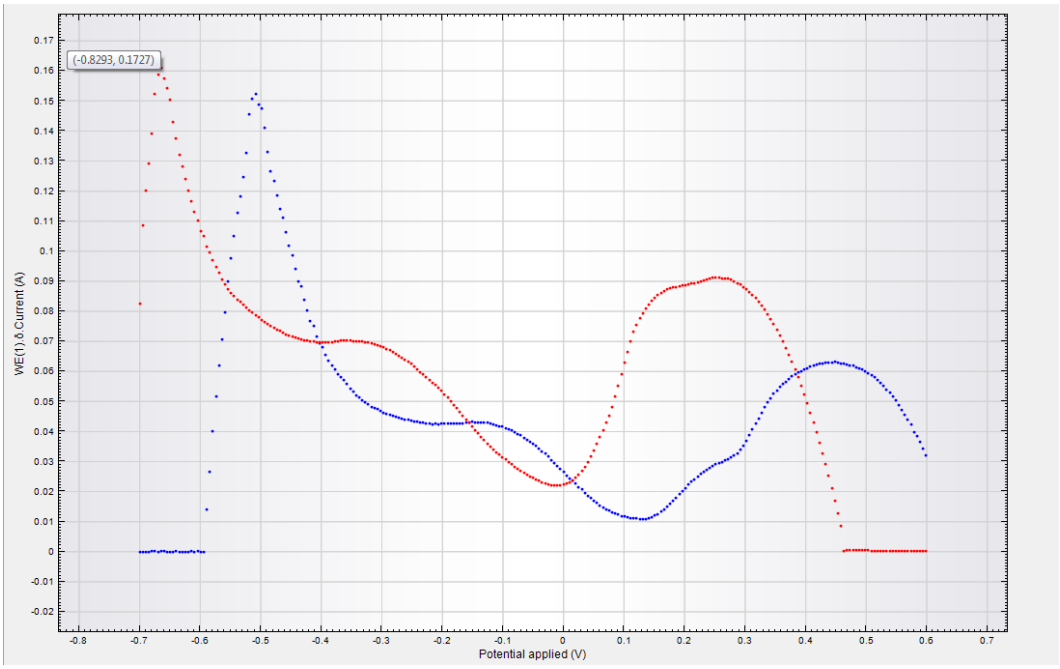

Figure 5.14. SWV data at 600ºC from the University of Wisconsin

collected salt samples for titration every 20 h. The temperatures ranged from 450 to 600°C. Figure 5.15 demonstrates how many moles of OH^- were titrated per gram of Solar Salt collected at different temperatures. It is clear that decomposition occurs at temperatures above 550°C, generating oxide ions and nitrites. Furthermore, these decompositions are time dependent.

Figure 5.16 shows that the probe produced at the University of Utah performs adequately and correlates to the titration data. SWV tests confirm the decomposition at the same temperature and show the time dependence. The correlation is seen in Figure 5.17. While it proves that it is possible to quantify the decomposition, a more advanced titration method is needed to differentiate between oxide and nitrite ions.

Table 5.2. Timeline of sample and data collection

Sample ID	Temperature, °C	Date of collection
1	450	9/26/2015
2	450	9/26/2015
3	500	9/27/2015
4	500	9/27/2015
5	565	9/28/2015
6	565	9/29/2015
7	585	9/29/2015
8	585	9/30/2015
9	600	10/1/2015
10	600	10/2/2015

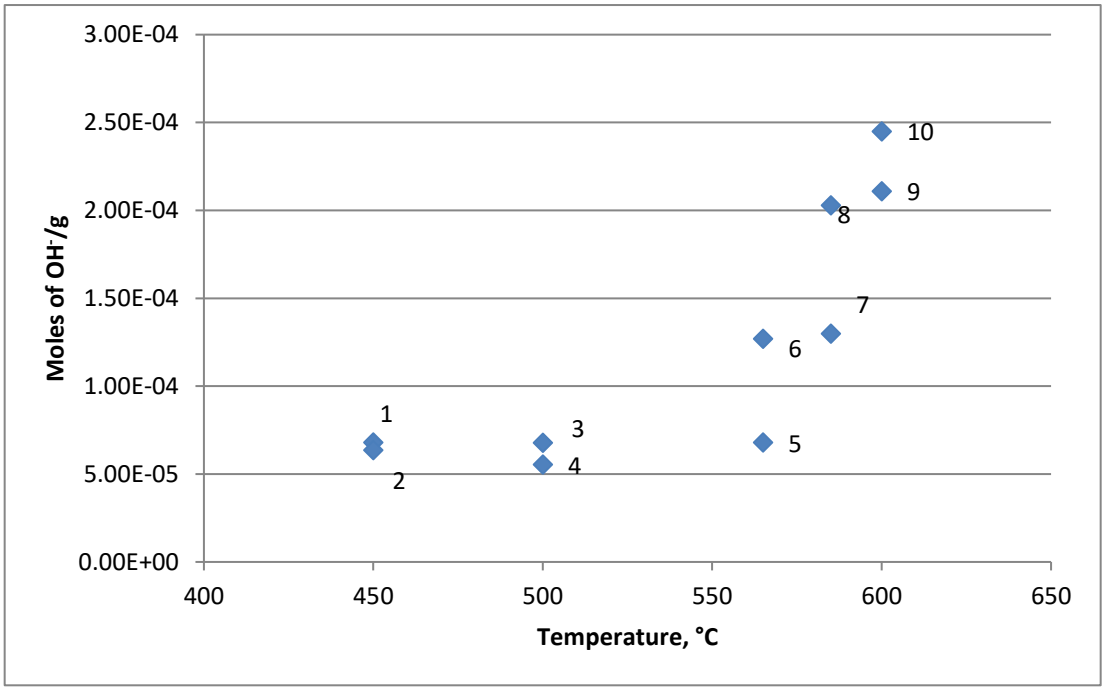

Figure 5.15. Moles of OH^- titrated per gram of Solar Salt

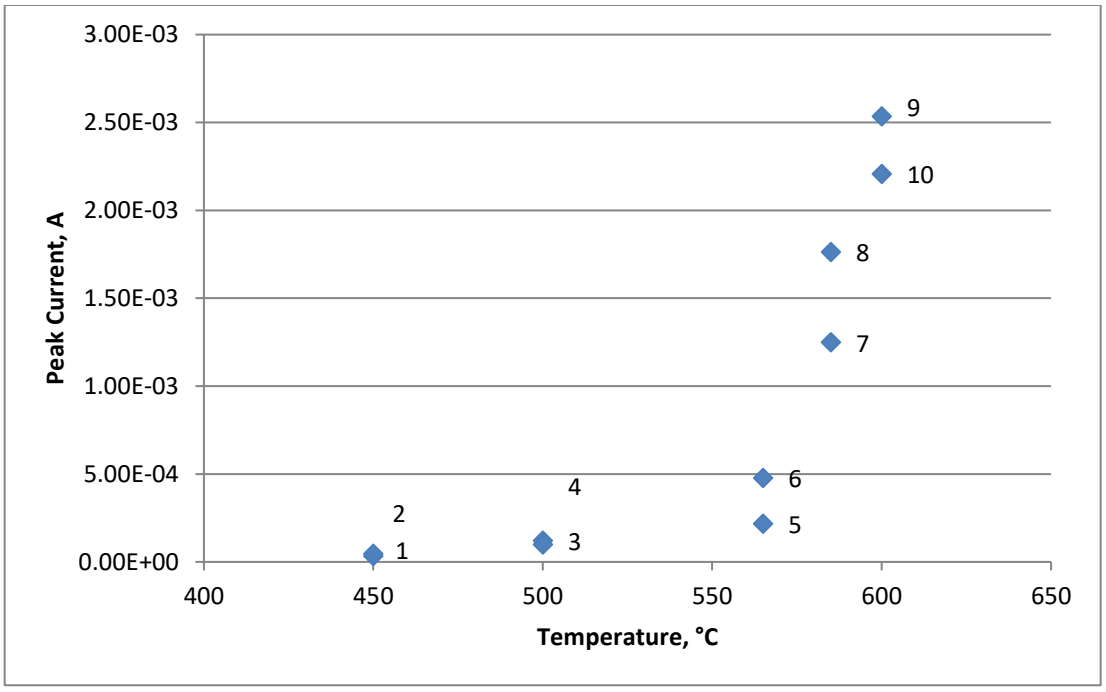

Figure 5.16. Peak current values with temperature increase

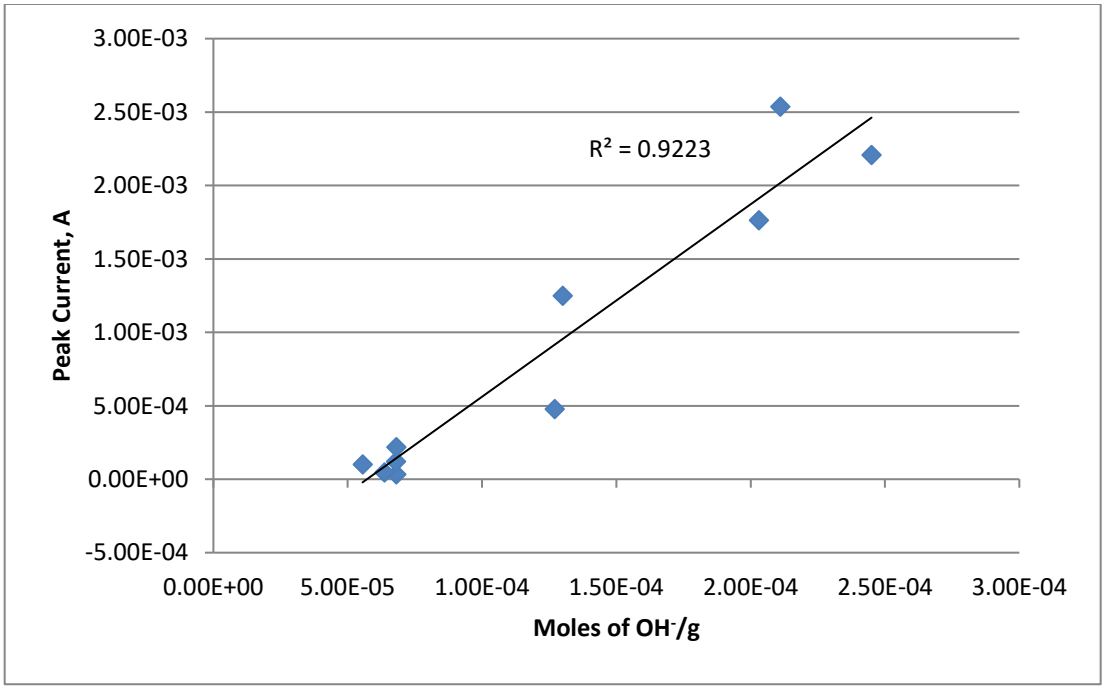

Figure 5.17. Correlation of titration measurements and SWV readings

CHAPTER 6

CONCLUSIONS

This project was focused on the use of electrochemical analysis methods to quantitatively measure the physical state of molten nitrate salts that are considered candidates for use as heat transfer fluids in concentrated solar power plants. The decomposition of the salt at high temperatures is of concern, which should correlate with the presence of oxide ions in the salt. The problem is that there is no established real-time method for directly measuring oxide ions in molten salt. Using established electrochemical principles and test methods, a variety of electrochemical test methods and test materials were investigated in this project to support development of a real-time sensor for oxide ions in molten nitrate salts.

It was observed that three-electrode direct current (DC) voltammetry methods including cyclic voltammetry (CV), linear sweep voltammetry (LSV), and square wave voltammetry (SWV) generate output that is responsive to changes in the O^{2-} concentration in both nitrate salts that were studied in this project – HITEC and Solar Salt. Multiple calibration curves for oxide ion concentration versus peak current were developed in bench scale electrochemical experiments, and an electrochemical sensor configuration was invented for measuring oxide ion concentrations in molten salts used in large-scale solar energy systems.

It was found that each salt had to be evaluated specifically to determine the optimal procedure for oxide ion measurement. CV with a wide range of potentials is run first to identify anodic and cathodic peaks. Referring to literature and other known aspects of the salt, these peaks are then identified based on specific oxidation or reduction reactions. This can inform the final decision about which method is best suited to O^{2-} analysis. For HITEC, it was determined that linear sweep voltammetry (LSV) was the best technique to observe the changes in a peak that represents an electrochemical reaction between nitrite and oxide ions. Since concentrations of both ions contribute to the peak height, and the concentration of nitrites is relatively constant, major peak height changes were contributed to the changes in oxide concentration. Square wave voltammetry (SWV) was chosen for Solar Salt due to its high sensitivity. Solar Salt does not contain nitrites, so the peak used for HITEC could not be used. Rather, it was necessary to quantify a very small O^{2-} oxidation peak. SWV excels at low concentrations or low peak intensities. The height of the measured SWV peaks divided by the surface area of the electrode were correlated via a linear function to the oxide ion concentration. Once calibration curves were developed, peak heights could be directly used to analyze oxide ion concentrations.

However, there are problems with these nitrate salts that complicate the interpretation of experimental measurements. These salts start to decompose within the temperature range at which calibration measurements need to be made. This complicates the development of calibration curves, since the O^{2-} concentration might actually change during the process of making a measurement. While there is a titration method to determine O^{2-} concentration in a sample of the salt via wet chemical analysis, nitrites actually interfere with the measurement. Both nitrites and oxides contribute to formation

of hydroxide ion during the aqueous titration. This makes it hard to confirm the as-prepared oxide ion concentration in the salt. Since the current response from voltammetry should be invariant at constant surface area and O^{2-} concentration, voltammetry could still be used to track relative changes in the O^{2-} concentration. This would require near continuous operation of the voltammetry probe.

The probe designed and assembled based on this study performed effectively to measure the increase in oxide concentrations during a weeklong test at the University of Wisconsin. Platinum coated titanium rods are a great alternative to costly and fragile platinum wire. The novel use of thin-walled mullite instead of Pyrex glass tubes for reference electrode prolonged the use of the electrode and made it a lot more resistant to thermal shock. Sensors with similar design could be used in various molten salt applications to continuously monitor the concentration of oxide ions.

In summary, electrochemical measurements give a great insight in the behavior of HITEC and Solar Salt. Using various modifications of probe design and voltammetry settings, it is possible to measure concentrations of other ions. To improve the quality of calibration curves, more experiments should be conducted with a wider range of temperatures and different concentrations of ions. Lab grade salt mixtures with no impurities will also decrease the error and improve the quality of data. And advanced titration techniques will help differentiate between the concentration of nitrite and oxide ions in the salt samples. These are just some of the areas of further study that should be pursued in the future to optimize this voltammetry application and facilitate its implementation in commercial solar power plants.

REFERENCES

1. Tomar, A.; Jain, L.; Batra, P.; Shirbhate, M. R. S.; Bhandari, G.; Singh, B.; Singh, K.; Borkar, M.; Nayyar, V.; Akhai, S. Solar Energy-Finding New Ways. *Int. J. Res. Advent Tech.* **2013,** *1*, 1-2.

2. Green, M. A. Photovoltaic Principles. *Phys. E (Amsterdam, Neth.)* **2002,** *14* (1), 11-17.

3. Ragheb, M. Solar Thermal Power and Energy Storage Historical Perspective, 2014. Nuclear Power Engineering. http://mragheb.com/NPRE%20498ES%20Energy%20Storage%20Systems/index.htm (accessed Jan 5, 2016).

4. Chapin, D. M.; Fuller, C.; Pearson, G. A New Silicon p-n Junction Photocell for Converting Solar Radiation into Electrical Power. *J. Appl. Phys. (Melville, NY, U. S.)* **1954,** *25* (5), 676-677.

5. Buck, A. L. *A History of the Energy Research and Development Administration*. US Department of Energy, Assistant Secretary, Management and Administration, Office of the Executive Secretariat, U.S. Government Printing Office: Washington, DC, 1982.

6. Concentrating Solar Power. US Department of Energy, http://energy.gov/eere/sunshot/concentrating-solar-power (accessed Jan 5, 2016).

7. Linear Concentrator System Basics for Concentrating Solar Power. Energy.gov, http://energy.gov/eere/energybasics/articles/linear-concentrator-system-basics-concentrating-solar-power (accessed Jan 5, 2016).

8. Concentrating Solar Power Tower System Basics. Energy.gov, http://energy.gov/eere/energybasics/articles/concentrating-solar-power-tower-system-basics (accessed Jan 5, 2016).

9. Vignarooban, K.; Xu, X.; Arvay, A.; Hsu, K.; Kannan, A. Heat Transfer Fluids for Concentrating Solar Power Systems–a Review. *Appl. Energy.* **2015,** *146*, 383-396.

10. California Energy Commission. *ISEGS Order Approving Petition to Amend*; 2014.

11. Tessera Solar and Stirling Energy Systems Unveil World's First Commercial Scale

Suncatcher TM Plant, Maricopa Solar, with Utility Partner Salt River Project, 2010. Press Release, Tessera Solar. http://tesserasolar.com/north-america/pdf/2010_01_22.pdf (accessed Jan 5, 2016).

12. Concentrating Solar Power Dish/Engine System Basics. Energy.gov, http://energy.gov/eere/energybasics/articles/concentrating-solar-power-dishengine-system-basics (accessed Jan 5, 2016).

13. Kearney, D.; Herrmann, U.; Nava, P.; Kelly, B.; Mahoney, R.; Pacheco, J.; Cable, R.; Potrovitza, N.; Blake, D.; Price, H. Assessment of a Molten Salt Heat Transfer Fluid in a Parabolic Trough Solar Field. *J. Sol. Energy Eng.* **2003,** *125* (2), 170-176.

14. Bradshaw, R. W.; Siegel, N. P. In *Molten Nitrate Salt Development for Thermal Energy Storage in Parabolic Trough Solar Power Systems,* ASME 2008 2nd International Conference on Energy Sustainability collocated with the Heat Transfer, Fluids Engineering, and 3rd Energy Nanotechnology Conferences, American Society of Mechanical Engineers, Jacksonville, FL, Aug 10-14, 2008.

15. Coastal Chemical Co., L.L.C. HITEC ® Heat Transfer Salt. Stoppingclimatechange.com. http://stoppingclimatechange.com/MSR%20-%20HITEC%20Heat%20Transfer%20Salt.pdf (accessed Jan 5, 2016).

16. Carling, R.; Kramer, C.; Bradshaw, R.; Nissen, D.; Goods, S.; Mar, R.; Munford, J.; Karnowsky, M.; Biefeld, R.; Norem, N. *Molten Nitrate Salt Technology Development Status Report*; SAND80-8052; Sandia National Laboratories, Livermore, CA; Sandia National Labs.: Albuquerque, NM, 1981.

17. Bauer, T.; Breidenbach, N.; Pfleger, N.; Laing, D.; Eckand, M. In *Overview of Molten Salt Storage Systems and Material Development for Solar Thermal Power Plants*, National Solar Conference and World Renewable Energy Forum 2012, Denver, CO, May 13-19, 2012.

18. Kruizenga, A.; Cordaro, J. G. *Preliminary Development of Thermal Stability Criterion for Alkali Nitrates*; SAND2011-5837C; Sandia National Laboratories, Livermore, CA; Sandia National Labs.: Livermore, CA, 2011.

19. Reilly, H. E.; Kolb, G. J. *An Evaluation of Molten-Salt Power Towers Including Results of the Solar Two Project*; SAND2001-3674; Sandia National Laboratories, Albuquerque, NM; Sandia National Labs: Livermore, CA, 2001.

20. Kelly, B.; Price, H.; Brosseau, D.; Kearney, D. In *Adopting Nitrate/Nitrite Salt Mixtures as the Heat Transport Fluid in Parabolic Trough Power Plants*, ASME 2007 Energy Sustainability Conference, American Society of Mechanical Engineers, Long Beach, CA, 2007.

21. Freeman, E. S. The Kinetics of the Thermal Decomposition of Sodium Nitrate and of the Reaction Between Sodium Nitrite and Oxygen. *J. Phys. Chem.* **1956,** *60* (11),

1487-1493.

22. Freeman, E. S. The Kinetics of the Thermal Decomposition of Potassium Nitrate and of the Reaction between Potassium Nitrite and Oxygen. *J. Am. Chem. Soc.* **1957,** *79* (4), 838-842.

23. Bagaratiyan, N.V.; Il'in, M.K.; Nikitin, O.T. *Mosc. Univ. Chem. Bull*. **1977**, *32* (10).

24. Bagaratiyan, N.V.; Nikitin, O.T. *Mosc. Univ. Chem. Bull*. **1977**, *32* (8).

25. Hatt, B. W. Industrial Organic and Fuel Chemistry. *Molten Salt Technology*, Springer: New York 1982; pp 395-455.

26. Jordan, J.; Mccarthy, W.; Zambonin, P.; Mamantov, G. Characterization and Analysis. *Molten Salts*. Academic Press: Cambridge, MA, 1969; pp 575-592.

27. Picard, G.; Flament, T.; Tremillon, B. Acidity and Thermochemical Stability of Molten Sodium Nitrate and Nitrite Mixtures. *J. Electrochem. Soc.* **1985,** *132* (4), 863-868.

28. Alexander Jr, J.; Hindin, S. Phase Relations in Heat Transfer Salt Systems. *Ind. Eng. Chem.* **1947,** *39* (8), 1044-1049.

29. Bartholomew, R. F. A Study of the Equilibrium KNO3 (l)⇌ KNO2 (l)+ 1/2O2 (g) over the Temperature Range 550-750°. *J. Phys. Chem.* **1966,** *70* (11), 3442-3446.

30. Cases-Casanova, J. Contribution to the Study of the Thermolysis of Sodium Nitrate. M.S. Thesis, University of Paris, 1959.

31. Peneloux, A., Thermodynamique et Cinetique de la Decomposition des Nitrites Alcalins et Alcalinoterreux. *C. R. Hebd. Seances Acad. Sci.* **1953,** *237* (18), 1082-1084.

32. Al-Omer, S.; Kerridge, D. Molten Sodium Nitrite-Potassium Nitrite Eutectic; the Reactions of Vanadium Compounds. *Inorg. Chim. Acta.* **1973,** *7*, 665-668.

33. Choi, E.-Y.; Choi, I.-K.; Hur, J.-M.; Kang, D.-S.; Shin, H.-S.; Jeong, S. M. In Situ Electrochemical Measurement of O2− Concentration in Molten Li2O/LiCl during Uranium Oxide Reduction Process. *Electrochem. Solid-State Lett.* **2011,** *15* (3), E11-E13.

34. Massot, L.; Cassayre, L.; Chamelot, P.; Taxil, P. On the Use of Electrochemical Techniques to Monitor Free Oxide Content in Molten Fluoride Media. *J. Electroanal. Chem.* **2007,** *606* (1), 17-23.

35. Berghoute, Y.; Salmi, A.; Lantelme, F. Internal Reference Systems for Fused

Electrolytes. *J. Electroanal. Chem.* **1994,** *365* (1-2), 171-177.

36. Iizuka, M.; Inoue, T.; Shirai, O.; Iwai, T.; Arai, Y. Application of Normal Pulse Voltammetry to On-line Monitoring of Actinide Concentrations in Molten Salt Electrolyte. *J. Nucl. Mat.* **2001,** *297* (1), 43-51.

37. Bauer, T.; Laing, D.; Tamme, R. Recent Progress in Alkali Nitrate/Nitrite Developments for Solar Thermal Power Applications. *Molten Salts Chemistry and Technology* **2011**, 543-553.

38. Bard, A. J.; Faulkner, L. R. *Electrochemical Methods: Fundamentals and Applications*; Wiley: New York, 2001.

39. Stern, K. H. High Temperature Properties and Decomposition of Inorganic Salts Part 3, Nitrates and Nitrites. *J. Phys. Chem. Ref. Data.* **1972,** *1*, 747-772.